

# Analysis of kinetic-diffusion Monte Carlo simulation and source term estimation scheme in nuclear fusion applications

Zhirui Tang<sup>a,\*</sup>, Julian Koellermeier<sup>b,c</sup>, Emil Løvbak<sup>d,\*\*</sup>, Giovanni Samaey<sup>a,\*\*</sup>

<sup>a</sup>*Department of Computer Science, KU Leuven, Leuven, 3001, Belgium*

<sup>b</sup>*Bernoulli Institute, University of Groningen, Groningen, 9747, The Netherlands*

<sup>c</sup>*Department of Mathematics, Computer Science and Statistics, Ghent University, Gent, 9000, Belgium*

<sup>d</sup>*Scientific Computing Center, Karlsruhe Institute of Technology, Karlsruhe, 76131, Germany*

---

## Abstract

In plasma edge simulations, the behavior of neutral particles is often described by a Boltzmann–BGK equation. Solving this kinetic equation and estimating the moments of its solution are essential tasks, typically carried out using Monte Carlo (MC) methods. However, for large-sized reactors, like ITER and DEMO, high collision rates lead to a substantial computational cost. To accelerate the calculation, an asymptotic-preserving kinetic-diffusion Monte Carlo (KDMC) simulation method (Mortier et al., SIAM J. Sci. Comput., 2022) and a corresponding fluid estimation technique (Mortier et al., Contrib. Plasma Phys., 2022) have recently been proposed. In this work, we present a comprehensive analysis of the convergence of KDMC combined with the associated fluid estimation. The analysis consists of proving theoretical upper bounds for both KDMC and the fluid estimation, and numerical verifications of these bounds. In addition, we compare the analyzed algorithm with a purely fluid-based method using the fully kinetic MC method as a reference. The algorithm consistently achieves lower error than the fluid-based method, and even one order of magnitude lower in a fusion-relevant test case. Moreover, the algorithm exhibits a significant speedup compared to the reference kinetic MC method. Overall, our analysis confirms the effectiveness of KDMC with the associated fluid estimation in nuclear fusion applications.

*Keywords:* error analysis, kinetic-diffusion Monte Carlo, Boltzmann–BGK, moment estimation

---

## 1. Introduction

Kinetic equations are widely used to model the behavior of particles in various physical systems, such as radiation transport [1], rarefied gas dynamics [2], and nuclear fusion [3, 4]. In these applications, the collision rate of particles may be high, requiring a huge amount of computational resources. In this case, approximate fluid models can be used to speed up the simulation without too much loss of accuracy [5, 6]. Nevertheless, situations where the collision rates vary dramatically across the simulation domain result in the fluid model being inaccurate in low-collision regimes, while the kinetic model remains inefficient in high-collision regimes.

There are three main approaches for handling the above situation. The first one is domain decomposition [7, 8, 9], where the simulation domain is divided into a kinetic and a fluid part, and different methods are applied to each part. A second approach, rather than decomposing the domain, is to decompose the solution itself into a kinetic part and a fluid part [10, 11, 12]. Both approaches face problems of how to decompose either the domain or the distribution function. The efficiency and accuracy of both approaches strongly depend on the quality of the decomposition. A third approach is provided by the asymptotic-preserving method, avoiding the need for an explicit decomposition by employing a single adaptive method, see e.g., [13, 14, 15, 16]. Our main interest lies in asymptotic-preserving Monte

---

\*Corresponding author: zhirui.tang@kuleuven.be

\*\*These authors contributed equally and share senior authorship.

<sup>1</sup>This paper significantly extends a previously submitted short article by Tang et al. (2025), which reported preliminary numerical results that are used in Section 5.6 of this work.

Carlo (APMC) methods [17, 18, 19, 20]. Using Monte Carlo (MC) enables APMC to be dimension-independent, facilitates handling complex geometries, and prevents the need to fully resolve the velocity domain. This work is based on the recently designed APMC method, known as kinetic-diffusion MC (KDMC) [17].

The works mentioned above focus on the solution of the kinetic model, but this solution is not always the final quantity of interest. For instance, in plasma edge simulations, the primary focus is often placed on the first three moments of the particle distribution function, which describe the density of ionized particles, and the amount of transferred momentum and energy [21, 22]. KDMC approximates the solution of the kinetic model by generating discrete particle trajectories. Based on these trajectories, [23] proposes a fluid estimation procedure for estimating the moments. As the main contribution in this work, we analyze KDMC and the associated fluid estimation procedure. The analysis is performed in one dimension for simplicity; however, all derivations remain valid in higher dimensions.

The analysis is divided into two parts. The first part is on the convergence of the KDMC simulation, with the standard MC (also called the kinetic MC) method used as a benchmark. The 1-Wasserstein distance is employed to compare the distributions generated by the standard MC and the KDMC simulations. The original work [17] contains an analysis based on the assumption that the particle motion is conditioned by fixed parameters, and a sharp error bound is derived. However, in practical simulations, these conditions are difficult to satisfy, making the convergence challenging to observe. In this work, we propose an alternative analysis that does not rely on fixed parameter assumptions. Although the resulting error bound is comparatively looser, the corresponding convergence is clearly observed in numerical experiments. Furthermore, our analysis demonstrates a property of KDMC that the error is small in low- and high-collision regimes, and relatively large in the intermediate regime.

The second part addresses the estimation error. The estimation consists of the kinetic part estimated by the standard MC method and the diffusive part estimated by the fluid estimation procedure. The estimation error is first decomposed into the kinetic and the diffusive parts, each analyzed separately. The estimation error of the kinetic part, affected by parameters in KDMC, is purely statistical, as standard MC is unbiased. The estimation error of the diffusive part arises from multiple sources, including statistical and deterministic errors, and therefore a bias exists.

In numerical experiments, we illustrate each error individually. Due to the design of KDMC, the errors impact each other. Hence, we propose dedicated experiments to isolate these errors. KDMC, which is based on the hybridization of the standard MC method and a fluid-based method, is expected to offer higher computational efficiency than the former while achieving greater accuracy than the latter. To demonstrate this, the algorithm is compared with the fluid-based method, using the standard MC as a reference. The comparison is carried out on a homogeneous background test case and a fusion-relevant heterogeneous test case. Subsequently, the computational efficiency of the algorithm is evaluated against that of the standard MC, and a speed-up rate is derived.

The remainder of the paper is organized as follows. The theoretical background, including the underlying kinetic equation, the fluid model, the KDMC algorithm, and the fluid estimation, is introduced in Section 2. The simulation error is discussed in Section 3, followed by the estimation error in Section 4. The numerical experiments are presented in Section 5. Finally, in Section 6, we conclude the work and give an outlook on future research.

## 2. KDMC simulation and fluid estimation

This section introduces KDMC and the associated fluid estimation, together with the theoretical background required for the subsequent analysis. We begin in Section 2.1 with the kinetic equation governing neutral particles at the plasma edge. Based on appropriate scaling assumptions, we introduce a fluid model (also known as the fluid limit) of the kinetic equation in Section 2.2. The KDMC method and the fluid estimation, both relying on this fluid model, are then described in Sections 2.3 and 2.4, respectively.

### 2.1. Boltzmann-BGK equation for neutral particles

In nuclear fusion applications, neutral particles can be modeled using the steady-state Boltzmann equation with the BGK operator [11]. In computer simulations, however, a time-dependent Boltzmann-BGK equation is used if a particle-based method (such as the standard MC or KDMC) is applied, since there is no steady-state behavior for a single particle, and the system evolves toward the steady-state from an initial state. In Appendix A, two time-dependent simulations, the terminal-time and the time-integrated simulations, are compared to validate the simulation of the steady-state system by the time-dependent model. In this work, we focus on the one-dimensional time-dependent

Boltzmann-BGK equation describing the transport of neutrals driven by the collisions between neutrals and plasma, which reads

$$\partial_t f(x, v, t) + v \partial_x f(x, v, t) = R(x) \left( M_p(v|x) \int_{-\infty}^{\infty} f(x, v', t) dv' - f(x, v, t) \right), \quad (1)$$

with the initial condition  $f(x, v, 0) = S(x, v)$ . Here,  $f(x, v, t)$  is the distribution of the neutral particles at position  $x$  with velocity  $v$  at time  $t$ , and  $S(x, v)$  is a neutral particle source from plasma recombination. We consider only the charge-exchange collision, in which neutrals are scattered and acquire new velocities. The collision rate is given as  $R(x)$ . The normalized drifting Maxwellian distribution is

$$M_p(v|x) = \frac{1}{\sqrt{2\pi\sigma_p^2(x)}} \exp\left(-\frac{1}{2} \frac{(v - u_p(x))^2}{\sigma_p^2(x)}\right), \quad (2)$$

a normal distribution with mean  $u_p(x)$  and variance  $\sigma_p^2(x) = T(x)/m$ , where  $u_p(x)$  and  $T(x)$  are the mean velocity and the temperature of plasma, respectively. The constant  $m$  is the mass of an ion.

Instead of the distribution  $f(x, v, t)$ , one is typically interested in the mass, momentum, and energy sources (from the neutrals to the plasma), in which the main components are three time-integrated moments, defined as

$$m_0(x) = \int_0^{\bar{t}} \int_{-\infty}^{\infty} f(x, v, t) dv dt, \quad m_1(x) = \int_0^{\bar{t}} \int_{-\infty}^{\infty} v f(x, v, t) dv dt, \quad \text{and} \quad m_2(x) = \int_0^{\bar{t}} \int_{-\infty}^{\infty} \frac{v^2}{2} f(x, v, t) dv dt. \quad (3)$$

The time integration up to the final time  $\bar{t} = \infty$  is consistent with the time-integrated simulation, which, as shown in Appendix A, yields lower errors than the time-terminal simulation. This simulation also aligns with the strategy used in the EIRENE code [24] (see the “Unbiased Estimators” section of its user manual). Correspondingly, we adopt the time-integrated quantity throughout this work. In what follows, we refer to the process of obtaining a discrete representation of the distribution  $f(x, v, t)$  as simulation, while the calculation of moments (3) is termed estimation.

## 2.2. Diffusive scaling and fluid limit

In large-scale nuclear fusion devices, like ITER, the collision rate in certain regions of the plasma edge is relatively high, and the distribution of the neutral particles is close to equilibrium, which enables the approximation of the Boltzmann-BGK equation by a fluid model.

The fluid model can be derived by the diffusive scaling assumption with an asymptotic expansion [5, 6, 11]. Specifically, we assume that the quantities of the simulation background scale with a small parameter  $\varepsilon$ , and the solution of (1) can be expanded as  $f(x, v, t) = f_0(x, v, t) + \varepsilon f_1(x, v, t) + \varepsilon^2 f_2(x, v, t) + \dots$ .

In the so-called diffusive scaling, we assume that the velocity of an individual plasma particle,  $v_p \sim O(1/\varepsilon)$ , is high, while the mean plasma velocity,  $u_p(x) \sim O(1)$ , is relatively low. This difference leads to the velocity variance of the plasma  $\sigma_p^2(x) = \int (v_p - u_p(x))^2 M_p(v|x) dv \sim O(1/\varepsilon^2)$ . In the high-collisional regime, the neutral particles are close to the equilibrium of the plasma particles, so the velocity of a neutral particle  $v$  has the same order of magnitude as  $v_p$ . In addition, collisions with the rate  $R \sim O(1/\varepsilon^2)$  dominate in this regime, meaning that particles collide frequently. A detailed description can be found in [6].

Based on the above diffusive scaling assumptions, taking the first order truncated expansion  $f_f(x, v, t) = f_0(x, v, t) + \varepsilon f_1(x, v, t)$ , and applying the Hilbert expansion [25], we obtain the fluid model

$$\partial_t \rho(x, t) + \partial_x \left( u_p(x) \rho(x, t) \right) - \partial_x \left( \frac{1}{R(x)} \partial_x \left( \sigma_p^2(x) \rho(x, t) \right) \right) = 0, \quad (4)$$

where  $\rho(x, t) = \int_{-\infty}^{\infty} f_f(x, v, t) dv$  is the density of particles. The full derivation can be found in [6]. Substituting the truncated expansion  $f_f(x, v, t)$  into moments (3), we have

$$m_0(x) \approx \int_0^{\bar{t}} \rho(x, t) dt, \quad (5)$$

$$m_1(x) \approx \int_0^{\bar{t}} \rho(x, t) u_p(x) - \frac{1}{R(x)} \partial_x \left( \sigma_p^2(x) \rho(x, t) \right) dt, \quad (6)$$

$$m_2(x) \approx \int_0^{\bar{t}} \frac{1}{2} \left( u_p^2(x) + \sigma_p^2(x) \right) \rho(x, t) - \frac{1}{R(x)} \partial_x \left( u_p(x) \sigma_p^2(x) \rho(x, t) \right) dt, \quad (7)$$

where  $\rho(x, t)$  is the solution of (4). The approach that estimates the moments (3) by solving the fluid model (4) and calculating (5)–(7) is referred to as the fluid-based method or simply the fluid method. In Section 4.3, we demonstrate that the approximate moments (5)–(7) differ from the true moments (3) by an error of order  $O(\varepsilon^2)$ . We call this error the model error.

### 2.3. Kinetic-Diffusion Monte Carlo

In this section, we introduce the simulation methods used in this work for computing the particle distribution  $f(x, v, t)$  described by the Boltzmann-BGK equation (1). We begin in Section 2.3.1 with the standard MC method, referred to as the kinetic simulation. In Section 2.3.2, we present a diffusion simulation based on the fluid model (4). Finally, in Section 2.3.3, we introduce KDMC, which hybridizes the kinetic and the diffusion simulations.

#### 2.3.1. Kinetic simulation

With an MC method, the time-integrated particle distribution is approximated by summing Dirac measures associated with the discretized trajectory of particles. To simulate the discretized trajectories, we consider the  $i$ -th particle with  $i = 1, 2, \dots, I$  with weight  $w_i$ , where  $I$  is the number of particles. The weight indicates the fraction of the total mass that the particle represents for the system. In particular, if the system has the initial density  $\rho(x, t = 0)$ , the weight  $w_i = \int \rho(x, t = 0) dx / I$  for all  $i$ . Next, the simulation of this particle starts from the time  $t = 0$  at the position  $x_i^0$  with the velocity  $v_i^0$ . After a flight time  $\tau$  sampled from the exponential distribution  $\text{Exp}(R(x_i^0))$ , a charge-exchange collision occurs. At this point, the position of the particle updates to

$$x_i^1 = x_i^0 + \tau v_i^0, \quad (8)$$

and the particle is assigned a new velocity  $v_i^1$  sampled from the Maxwellian distribution  $M(v|x_i^1)$  given in (2). The movement (8) is called a kinetic step. Repeating the process up to the end of the simulation time  $\bar{t}$ , we obtain its trajectory denoted as  $\{(x_i^k, v_i^k)\}_{k=0}^{K_i}$ , where  $K_i$  is the total number of states of the  $i$ -th particle. The distribution obtained from the kinetic simulation in this section can then be assembled as in (13), using the trajectories of all particles.

#### 2.3.2. Diffusion simulation

Starting from the fluid model (4), we add and subtract the term  $\partial_x \left( \partial_x \left( \frac{1}{R(x)} \right) \sigma_p^2(x) \rho(x, t) \right)$  on the left-hand side, such that the fluid model becomes

$$\partial_t \rho(x, t) + \partial_x \left( \left( u_p(x) + \partial_x \left( \frac{1}{R(x)} \right) \sigma_p^2(x) \right) \rho(x, t) \right) - \partial_{xx} \left( \frac{\sigma_p^2(x)}{R(x)} \rho(x, t) \right) = 0, \quad (9)$$

a Fokker-Plank equation [26]. Its Ito stochastic differential equation (SDE) is

$$dX_t = \left( u_p(X_t) + \partial_x \left( \frac{1}{R(X_t)} \right) \sigma_p^2(X_t) \right) dt + \sqrt{2 \frac{\sigma_p^2(X_t)}{R(X_t)}} dW_t. \quad (10)$$

with  $W_t$  a Brownian motion. Let

$$A(x) = u_p(x) + \partial_x \left( \frac{1}{R(x)} \right) \sigma_p^2(x) = u_p(x) + \frac{\partial D(x)}{\partial R(x)} \frac{\partial R(x)}{\partial x}, \quad \text{and} \quad D(x) = \frac{\sigma_p^2(x)}{R(x)}.$$

Applying the Euler-Maruyama approximation, this SDE indicates that the new position that the  $i$ -th particle travels a time  $\Delta t$  from  $x_i^k$  is

$$x_i^{k'} = x_i^k + A(x_i^k) \Delta t + \sqrt{2 D(x_i^k) \Delta t} \xi, \quad (11)$$

with  $\xi \sim \mathcal{N}(0, 1)$ . The movement (11) is called a diffusive step. When the scaling parameter  $\varepsilon \rightarrow 0$ , the true particle movement following Eq. (1) converges to this step.

### 2.3.3. Kinetic-Diffusion simulation

The kinetic simulation described in Section 2.3.1 is unbiased [27] but computationally expensive in highly collisional regimes. In contrast, the diffusion simulation introduced in Section 2.3.2 offers a significant reduction in computational cost in these regimes, with only a minor loss in accuracy. However, in low-collisional regimes, the fluid model (4) and thus the diffusion simulation no longer provides a good approximation, whereas the kinetic simulation is both valid and efficient. In the intermediate regime, one must choose between accuracy and efficiency.

These issues are handled in [17] by combining the advantages of the kinetic and the diffusion simulations. Specifically, we fix a time step size  $\Delta t$ . Consider the  $i$ -th particle. Within this time interval, the particle executes first a kinetic step (8) with time  $\tau$  and then a diffusive step (11) with  $\theta = \Delta t - \tau$ . If the flight time of the kinetic step  $\tau > \Delta t$ , no collision and diffusive step happens within the  $\Delta t$ . Only the kinetic step is performed. Intuitively, when the collision rate is high, i.e.,  $\tau \ll \Delta t$  on average, the particle will first perform a short kinetic step and then a dominant diffusive step for the rest of the time of size  $\Delta t$ . On the contrary, when the collision rate is low, i.e.,  $\tau \gg \Delta t$  on average, particles are primarily simulated by the kinetic step, and the influence of the inexact diffusive step is insignificant. In both situations, at most two flights happen per time step of size  $\Delta t$ , and the simulation has only a small bias.

Simulating the particle from  $t = 0$  to  $\bar{t} = K\Delta t$ , with  $K$  the number of time steps, we obtain the trajectory of the  $i$ -th particle as

$$\{(x_i^0, v_i^0), (x_i^{0'}, v_i^{0'}), (x_i^1, v_i^1), (x_i^{1'}, v_i^{1'}), \dots, (x_i^K, v_i^K), (x_i^{K'}, v_i^{K'})\}. \quad (12)$$

The state  $(x_i^k, v_i^k)$  with the index  $k$  is the starting state of the  $k$ -th kinetic step, and the state  $(x_i^{k'}, v_i^{k'})$  with the index  $k'$  is that of the  $k$ -th diffusive step, where  $k = 0, 1, \dots, K$ . The weight  $w_i = \int \rho(x, t=0) dx / I$  for all  $i$  as stated in Section 2.3.1. Repeating the above random process for all  $I$  particles, the time-integrated distribution can be expressed as the Klimontovich distribution [12]

$$f(x) = \int_0^{\bar{t}} \int_{-\infty}^{\infty} f(x, v, t) dv dt \approx \sum_{i=1}^I \sum_{k=0}^K w_i \delta(x - x_i^k) + \sum_{i=1}^I \sum_{k=0}^K w_i \delta(x - x_i^{k'}). \quad (13)$$

The algorithm is illustrated graphically in Figure 1. The corresponding pseudocode, including the fluid estimation procedure described in Section 2.4, is presented in Algorithm 1. The analysis of KDMC is provided in Section 3.

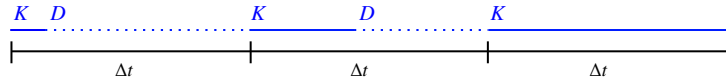


Figure 1: Illustration of KDMC. In the first time step of size  $\Delta t$ , the particle is in a high-collision regime such that the kinetic (K) step only lasts a short time and the diffusive (D) step dominates. In the third time step of size  $\Delta t$ , the particle is in a low-collisional regime where only the K step is performed.

### 2.4. Fluid estimation procedure for KDMC

After the simulation, we calculate/estimate the moments (3) based on the trajectories generated during the simulation (12). The contribution of the kinetic steps from  $(x_i^k, v_i^k)$  to  $(x_i^{k'}, v_i^{k'})$  can be estimated by MC estimators [27]. In our case, the moments (3) can be estimated as

$$m_l(x) = \int_0^{\bar{t}} m_l(x, t) dt = \int_{-\infty}^{\infty} s_l(x, v) f(x, v) dv \approx \frac{1}{I} \sum_{i=1}^I \sum_{k=0}^K s_l(x_i^k, v_i^k, x_i^{k'}, v_i^{k'}) \delta(x - x_i^k). \quad (14)$$

for  $l = 0, 1$ , and  $2$ , where  $s_l(x, v)$  are score functions [22] depending on the estimator, in other words, the estimating method. In this work, the track-length estimator [22] is applied. In fusion applications, discretization of the spatial domain is required [24]. The moments for the  $j$ -th cell  $C_j = [x_j, x_{j+1})$  are then

$$m_{l,j} = \int_{C_j} m_l(x) dx \approx \frac{1}{I} \sum_{i=1}^I \sum_{k=0}^K s_l(x_i^k, v_i^k, x_i^{k'}, v_i^{k'}) \mathbb{1}_{C_j}(x_i^k), \quad (15)$$

where  $\mathbb{1}_{C_j}(x)$  is the indicator function of the  $j$ -th cell. The process for obtaining the kinetic part of (13) is called the kinetic simulation, and the estimation method given by (15) is referred to as the MC estimator or the kinetic estimator.

For the diffusive simulation, in which the aggregate effect of many collisions is approximated with a single diffusive step, we only have incomplete trajectory information, and hence the MC estimator cannot produce a good estimate. To be specific, the position and velocity of each collision are required to produce unbiased estimates with the score function  $s_l(x, v)$  in the MC estimator (15), while only the starting and end positions are provided in a diffusive step (11). To address this issue, we make use of the fluid estimation procedure proposed in [23].

Since each diffusive step is designed to follow the particle-level dynamics of the fluid model (4) as discussed in Section 2.3.2, we then assume that the ensemble of all diffusive steps collectively approximates the macroscopic fluid governed by (4). The starting position of all diffusive steps gives the initial condition for the fluid motion. More precisely, the initial condition is

$$\hat{\rho}_0(x) = \sum_{i=1}^I \sum_{k'=0}^{K'_i} w_i \delta(x - x_i^{k'}), \quad (16)$$

where  $K'_i$  is the number of diffusive steps of the  $i$ -th particle. Then, the moments (3) are calculated by computing (5)-(7) after solving the fluid model (4) with the initial condition (16).

A challenge in the fluid estimation is that the durations of all diffusive steps over all particles are different. As a result, the evolution time of the fluid model, denoted as  $\theta$ , needs to be chosen in a sensible way. Here, we take  $\theta$  as the average duration of all diffusive steps. That is, if the flight time of  $i$ -th particle in the  $k$ -th diffusive step is  $\theta_i^k$ , the empirical evolution time

$$\hat{\theta} = \sum_{i=1}^I \sum_{k=0}^{K'_i} \frac{1}{I} \frac{1}{K'_i} \theta_i^k. \quad (17)$$

The error in the fluid estimation, along with the choice of the empirical evaluation time, is analyzed in Section 4.3. The complete algorithm of KDMC with the combined kinetic and fluid estimation described in this section is summarized in Algorithm 1, where the kinetic part and the fluid part moments are denoted as  $m^{\text{kinetic}}$  and  $m^{\text{fluid}}$ , respectively.

### 3. Error of Kinetic-Diffusion Monte Carlo Simulation

In this section, we derive an error bound for the KDMC simulation measured in the 1-Wasserstein ( $W_1$ ) distance. The standard MC method introduced in Section 2.3.1 is used as a reference solution. In Section 3.1, we introduce two definitions of the  $W_1$  distance in the one-dimensional case and explain its application by analyzing the movement of particles in the KDMC simulation. In Section 3.2, we derive a bound for the error of the KDMC simulation, focusing on two limit cases: the diffusive scaling parameter  $\varepsilon \rightarrow 0$  and the time step  $\Delta t \rightarrow 0$ . The KDMC simulation error is first derived at a fixed terminal time corresponding to the terminal-time simulation. Then, we demonstrate that the time-integrated simulation has a lower error.

#### 3.1. Wasserstein distance

To quantify the simulation error, we adopt the  $W_1$  distance [28] as our metric. Here, we introduce its two definitions for our one-dimensional case.

**Definition 3.1.** Let  $(X, d)$  be a metric space. For any two probability measures  $f, g$  on  $X$ , the  $W_1$  distance between  $f$  and  $g$  is defined as

$$W_1(f, g) = \inf \{ \mathbb{E}[d(X, Y)], \text{law}(X) = f, \text{law}(Y) = g \}. \quad (18)$$

The expectation  $\mathbb{E}$  of the metric  $d$  is

$$\mathbb{E}[d(X, Y)] = \iint d(x, y) f(dx) g(dy).$$

In our case, the law in (18) is the probability distribution of possible trajectories obtained from the kinetic or the KDMC simulation. Next, we explain how the particles' movement affects the  $W_1$  distance.

---

**Algorithm 1** KDMC simulation with the associated fluid estimation procedure

---

**Input:** Simulation time  $\bar{t}$ , time step  $\Delta t$ , number of particles  $I$ ,  
initial states  $(x_i^0, v_i^0)$  for  $i = 1, \dots, I$ .

**Output:** Moments  $m$

```

1:  $K \leftarrow \bar{t}/\Delta t$                                      ▷ Number of time steps
2: for  $i = 1$  to  $I$  do
3:   for  $k = 0$  to  $K - 1$  do
4:      $\tau \sim \text{Exp}(R(x_i^k))$ 
5:      $\tau \leftarrow \min(\tau, \Delta t)$                                 ▷ Time of kinetic step
6:      $x_i^{k'} \leftarrow x_i^k + \tau v_i^k$                       ▷ Kinetic step (Eq. (8))
7:      $\theta_i^k \leftarrow \max(\Delta t - \tau, 0)$                   ▷ Time of diffusive step
8:     if  $\tau < \Delta t$  then
9:       Sample  $v_i^{k'} \sim M(v|x_i^{k'})$  and  $v_i^{k+1} \leftarrow v_i^{k'}$   ▷ New velocity after collision
10:      Sample  $\xi \sim \mathcal{N}(0, 1)$ 
11:       $x_i^{k+1} \leftarrow x_i^{k'} + A(x_i^{k'})\theta_i^k + \sqrt{2D(x_i^{k'})\theta_i^k}\xi$   ▷ Diffusion step (Eq.(11))
12:      Store  $x_i^{k'}$  for the fluid estimation
13:    else                                                        ▷ If no diffusive step
14:       $x_i^{k+1} \leftarrow x_i^{k'}, v_i^{k'} \leftarrow v_i^k$ , and  $v_i^{k+1} \leftarrow v_i^k$ 
15:    end if
16:     $m^{\text{kinetic}} \leftarrow m^{\text{kinetic}} + \text{estimate}((x_i^k, v_i^k), (x_i^{k'}, v_i^{k'}))$   ▷ Kinetic part moments with MC estimator
17:    Store  $\theta_i^k$  for the fluid estimation
18:  end for
19: end for
20: Construct the initial condition  $\hat{\rho}_0(x)$  using all  $x_i^{k'}$  as Eq. (16).          ▷ Fluid estimation
21: Compute the empirical evolution time  $\hat{\theta}$  using all  $\theta_i^k$  as Eq. (17).
22: Solve the fluid model (4) with the initial condition  $\hat{\rho}_0(x)$  up to the time  $\hat{\theta}$ ,
    and estimate fluid part moments  $m^{\text{fluid}}$  as (5)-(7).
23: The total moments are given by  $m = m^{\text{kinetic}} + m^{\text{fluid}}$ .

```

---

Suppose the two empirical measures or simply distributions we compare are  $f(x)$  with its samples  $\{x_1, x_2, \dots, x_I\}$  and  $g(y)$  with its samples  $\{y_1, y_2, \dots, y_I\}$ , where  $f(x)$  is the reference distribution, and the samples are positions of particles. In the  $W_1$  distance, we need to find the minimal cost that moves particles sampled from  $g(y)$  such that  $g$  and  $f$  are identical distributions. A direct upper bound for  $W_1$  is found by moving  $y_i$  to  $x_i$  for all  $i = 0, 1, \dots, I$ , and the distance is  $\sum_i d(x_i, y_i)$ . Taking the metric  $d(x, y) = \|x - y\|_1$  and substituting into (18), we have

$$W_1(f, g) = \inf\{\mathbb{E}[\|x - y\|_1]\} \leq \lim_{I \rightarrow \infty} \frac{1}{I} \sum_{i=1}^I |x_i - y_i| \approx \frac{1}{I} \sum_{i=1}^I |x_i - y_i|. \quad (19)$$

The equality holds when  $x_i$  and  $y_i$  are sorted in ascending order in one-dimensional cases. The bound in (19) without sorting may overestimate the true  $W_1$  distance. In the error derivation of Section 3.2.2, some properties of the distributions are used to find a sharper upper bound than (19).

Alternatively, the  $W_1$  distance can be defined in terms of the cumulative distribution functions (CDF).

**Definition 3.2.** Suppose  $f(x)$  and  $g(x)$  are normalized probability distributions on  $\mathbb{R}$ , and  $F(x)$  and  $G(x)$  are their CDFs, respectively. The  $W_1$  distance between  $f(x)$  and  $g(x)$  is

$$W_1(f, g) = \int_{\mathbb{R}} |F(x) - G(x)| dx. \quad (20)$$

**Remark 1.** Both definitions apply to the so-called balanced problem, where the total mass of the two distributions  $f$  and  $g$  is equal. This condition holds in our application, as no particles disappear (i.e., no ionization) and no

new particles are born during the simulation. Consequently, the transport between  $f$  and  $g$  is mass-conserving, which ensures the well-posedness of the two definitions. Moreover, the distribution governed by the Boltzmann–BGK equation (1) is not necessarily normalized. Therefore, the distributions  $f(x)$  and  $g(x)$  should first be normalized for computing the  $W_1$  distance. For readability, we omit the explicit notation of this normalization in the manuscript.

### 3.2. Convergence of KDMC

We now derive the general expression of the  $W_1$  distance between the distributions generated from the kinetic and the KDMC simulations.

We denote the reference distribution obtained from the kinetic simulation at time  $t^{(k+1)} = (k+1)\Delta t$  as  $f(t^{(k+1)})$  and its approximation obtained from KDMC as  $f^{(k+1)}$ . If we define  $\mathcal{K}_{\Delta t}$  as the operator of applying the kinetic simulation to a distribution with one time step  $\Delta t$  and  $\mathcal{S}_{\Delta t}$  as that of the KDMC simulation, we have

$$f(t^{(k+1)}) = \mathcal{K}_{\Delta t}(f(t^{(k)})) \text{ and } f^{(k+1)} = \mathcal{S}_{\Delta t}(f^{(k)}).$$

Note that only one diffusive step (11) occurs in KDMC, whereas multiple kinetic steps (8) could happen in the single time step  $\Delta t$  in the kinetic simulation. The  $W_1$  distance between these two simulations at time  $t^{(k+1)}$  is then

$$\begin{aligned} W_1(f(t^{(k+1)}), f^{(k+1)}) &= W_1(\mathcal{K}_{\Delta t}(f(t^{(k)})), \mathcal{S}_{\Delta t}(f^{(k)})) \\ &\leq W_1(\mathcal{K}_{\Delta t}(f(t^{(k)})), \mathcal{K}_{\Delta t}(f^{(k)})) + W_1(\mathcal{K}_{\Delta t}(f^{(k)}), \mathcal{S}_{\Delta t}(f^{(k)})), \end{aligned} \quad (21)$$

where the triangle inequality of  $W_1$  distance [28] is applied. The first term in (21) is the difference of applying the reference scheme, that is, the kinetic simulation, to  $f(t^{(k)})$  and  $f^{(k)}$ , resulting in the different initial conditions to the time step. We show in Section 3.2.1 that this term is bounded by the global error at the previous time step  $t^{(k)}$ . The second term in (21) captures the error of performing one time step of the kinetic and the KDMC simulation on the same distribution  $f^{(k)}$ , and thus corresponds to the local error of KDMC compared to the kinetic simulation. This term is studied in Section 3.2.2, particularly in the limits:  $\varepsilon \rightarrow 0$ , and  $\Delta t \rightarrow 0$ . Finally, we provide a bound for the  $W_1$  distance between the kinetic and the KDMC simulations in Section 3.2.3.

#### 3.2.1. Global error term

This section shows that the first term in (21), i.e.,

$$W_1(\mathcal{K}_{\Delta t}(f(t^{(k)})), \mathcal{K}_{\Delta t}(f^{(k)})), \quad (22)$$

is bounded by  $W_1(f(t^{(k)}), f^{(k)})$ , which is the global error from the previous step. As a result, this term represents the propagation of the global error.

The expression (22) indicates the  $W_1$  distance between distributions produced by the kinetic simulation with the initial distributions  $f(t^{(k)})$  and  $f^{(k)}$ , respectively, up to time  $\Delta t$ . The kinetic simulation is unbiased, which means the resulting distribution represents the true solution of the Boltzmann–BGK equation (1) plus a statistical error that becomes negligible if a large enough number of particles is used. We first assume that an infinite number of particles is used so that the statistical error vanishes, and leave the discussion of statistical error to Section 3.2.3. With this assumption, the operator  $\mathcal{K}_{\Delta t}(f)$  is equivalent to evolving the initial distribution  $f$  with time  $\Delta t$  governed by the Boltzmann–BGK equation (1). Then, the following theorem shows that the operator  $\mathcal{K}_{\Delta t}$  is contractive under the  $W_1$  metric, thereby providing the error bound for (22).

**Theorem 3.1.** *Let  $f_0^1, f_0^2$  be two initial distributions of particles. With an infinite number of particles,  $f_{\Delta t}^1 = \mathcal{K}_{\Delta t}(f_0^1)$  and  $f_{\Delta t}^2 = \mathcal{K}_{\Delta t}(f_0^2)$  are corresponding solutions of the Boltzmann–BGK equation (1) at the time  $\Delta t$ . Then*

$$W_1(f_{\Delta t}^1, f_{\Delta t}^2) \leq W_1(f_0^1, f_0^2), \quad (23)$$

*Proof.* To prove this inequality, we first express the solution of the Boltzmann–BGK equation (1) as the so-called mild formulation [29] given by Duhamel’s principle, then apply the  $W_1$  distance on  $f_{\Delta t}^1$  and  $f_{\Delta t}^2$ . Afterwards, this inequality is obtained using Grönwall’s inequality. In this proof, we assume a homogeneous background  $R(x) = R$ . The argument

can, however, be performed in a heterogeneous background, for which the corresponding mild formulation can be found in Appendix B. Distributions, such as  $f_0^1$ , depend on  $(x, v)$ , and the dependency is written explicitly if necessary.

The mild formulation of the Boltzmann-BGK equation (1) (see Appendix B for the derivation) reads

$$f(x, v, t) = e^{-Rt} f_0(x - vt, v) + \int_0^t R e^{-R(t-s)} M_p[f](x - v(t-s), v, s) ds, \quad (24)$$

with

$$M_p[f](x, v, t) = M_p(v|x) \int_{-\infty}^{\infty} f(x, v', t) dv',$$

and the initial condition  $f(x, v, t = 0) = f_0(x, v)$ . Then,

$$f_{\Delta t}^i = e^{-R\Delta t} f_0^i(x - v\Delta t, v) + \int_0^{\Delta t} R e^{-R(\Delta t-s)} M_p[f^i](x - v(\Delta t-s), v, s) ds. \quad (25)$$

with  $i = 1, 2$ . In addition, we have

$$W_1(M_p[f^1], M_p[f^2]) \leq W_1(f^1, f^2),$$

since  $M[f]$  projects the full phase-space density  $f(x, v, t)$  onto a Maxwellian (in  $v$ ) that depends only on the local density  $\int f(x, v', t) dv'$  at time  $t$ . In other words, the projection  $f \mapsto M[f]$  smooths the distribution by removing the variation in  $v$ , and a lower cost is required to transport the distribution after the projection.

Next, applying the  $W_1$  distance on  $f_{\Delta t}^1$  and  $f_{\Delta t}^2$ , we have

$$W_1(f_{\Delta t}^1, f_{\Delta t}^2) \leq e^{-R\Delta t} W_1(f_0^1, f_0^2) + \int_0^{\Delta t} R e^{-R(\Delta t-s)} W_1(f_s^1, f_s^2) ds, \quad (26)$$

with the triangle inequality. We also use the fact that  $W_1(f_0^1(x - v\Delta t, v), f_0^2(x - v\Delta t, v)) = W_1(f_0^1(x, v), f_0^2(x, v))$  since the  $W_1$  metric is isometry invariant [30].

Finally, multiplying  $e^{R\Delta t}$  on both sides of (26) and by Grönwall's inequality [31], the inequality (26) becomes

$$e^{R\Delta t} W_1(f_{\Delta t}^1, f_{\Delta t}^2) \leq W_1(f_0^1, f_0^2) \exp\left(\int_0^{\Delta t} R e^{-R(\Delta t-s)} ds\right).$$

Further, we obtain

$$W_1(f_{\Delta t}^1, f_{\Delta t}^2) \leq W_1(f_0^1, f_0^2) \exp\left(1 - e^{-R\Delta t} - R\Delta t\right) \leq W_1(f_0^1, f_0^2). \quad \square$$

Substituting  $f_0^1 = f(t^{(k)})$ ,  $f_0^2 = f^{(k)}$ ,  $f_{\Delta t}^1 = \mathcal{K}_{\Delta t}(f(t^{(k)}))$ , and  $f_{\Delta t}^2 = \mathcal{K}_{\Delta t}(f^{(k)})$  into (23), we have

$$W_1(\mathcal{K}_{\Delta t}(f(t^{(k)})), \mathcal{K}_{\Delta t}(f^{(k)})) \leq W_1(f(t^{(k)}), f^{(k)}). \quad (27)$$

Substituting (27) into (21), we obtain

$$W_1(f(t^{(k+1)}), f^{(k+1)}) \leq W_1(f(t^{(k)}), f^{(k)}) + W_1(\mathcal{K}_{\Delta t}(f^{(k)}), \mathcal{S}_{\Delta t}(f^{(k)})). \quad (28)$$

This inequality states that the global error at the  $(k+1)$ -th time step is bounded by the error from the previous time step plus the local error introduced during the current step.

### 3.2.2. Local error term

In this section, we discuss the local error term

$$W_1(\mathcal{K}_{\Delta t}(f^{(k)}), \mathcal{S}_{\Delta t}(f^{(k)})), \quad (29)$$

in (21). The subsequent two theorems state that the local error term (29) is bounded by  $\mathcal{O}(\varepsilon^2)$  as the diffusive scaling parameter  $\varepsilon \rightarrow 0$  and  $\mathcal{O}(\Delta t^2)$  as the time step  $\Delta t \rightarrow 0$ , respectively.

**Theorem 3.2.** Let  $f^{(k)}$  be the distribution obtained from the KDMC simulation at time  $t^{(k)} = k\Delta t$ . Define  $\mathcal{K}_{\Delta t}$  as the operator of applying the kinetic simulation to a distribution with one time step  $\Delta t$  and  $\mathcal{S}_{\Delta t}$  as that of the KDMC simulation. As  $\varepsilon \rightarrow 0$ ,

$$W_1(\mathcal{K}_{\Delta t}(f^{(k)}), \mathcal{S}_{\Delta t}(f^{(k)})) \leq O(\varepsilon^2). \quad (30)$$

*Proof.* Denote  $f_k$  as the solution of (1) simulated by the kinetic simulation described in Section 2.3.1, and  $f_f$  as the solution of (4) simulated by the biased SDE (11), both evaluated at time  $t^{(k)}$ . To show that the local error term (29) is bounded by  $O(\varepsilon^2)$  as  $\varepsilon \rightarrow 0$ , we first find the  $W_1$  distance between  $f_k$  and  $f_f$ , and then bound (29) by this distance.

As mentioned in Section 2.2, the approximation error between the Boltzmann-BGK (1) and the fluid model (4) is  $O(\varepsilon^2)$ . Since  $f_k$  is the numerical solution of (1) with only the statistical error and  $f_f$  is the numerical solution of (11) with only the discretization error, we have  $|f_k - f_f| = O(\varepsilon^2)$ , if the statistical error and the discretization are assumed to be negligible. Assume the distribution be on the domain  $\Omega = [a, b]$ , then

$$F_k(x) - F_f(x) = \int_a^x f_k(y) - f_f(y) dy = O(\varepsilon^2),$$

where functions  $F_k$  and  $F_f$  are the CDFs of  $f_k$  and  $f_f$ , respectively. Further, the  $W_1$  distance between  $f_k$  and  $f_f$  is

$$W_1(f_k, f_f) = \int_a^b |F_k - F_f| dx = \int_a^b \left| \int_a^x f_k(y) - f_f(y) dy \right| dx = O(\varepsilon^2), \quad (31)$$

where the second definition of the  $W_1$  distance (20) is used.

If  $f_k$  is simulated with the initial distribution  $f^{(k)}$ , then  $f_k = \mathcal{K}_{\Delta t}(f^{(k)})$ . As for  $\mathcal{S}_{\Delta t}(f^{(k)})$ , it is obtained by a combination of the biased SDE (11) (diffusive step) and the unbiased kinetic simulation in Section 2.3.1 (kinetic step). Thus, the distance between  $\mathcal{S}_{\Delta t}(f^{(k)})$  and  $\mathcal{K}_{\Delta t}(f^{(k)})$  is less than the distance between  $f_k = \mathcal{K}_{\Delta t}(f^{(k)})$  and  $f_f$ , since  $f_f$  is simulated purely by the biased SDE. Consequently, the local error

$$W_1(\mathcal{K}_{\Delta t}(f^{(k)}), \mathcal{S}_{\Delta t}(f^{(k)})) \leq W_1(\mathcal{K}_{\Delta t}(f^{(k)}), f_f) = W_1(f_k, f_f) = O(\varepsilon^2). \quad \square$$

The following theorem provides a bound for the local error term (3.2.2) with respect to  $\Delta t$  as  $\Delta t \rightarrow 0$ .

**Theorem 3.3.** Let  $f(t^{(k)})$  be the distribution obtained from the kinetic simulation at time  $t^{(k)} = k\Delta t$ . Define  $\mathcal{K}_{\Delta t}$  as the operator of applying the kinetic simulation to a distribution with one time step  $\Delta t$  and  $\mathcal{S}_{\Delta t}$  as that of the KDMC simulation. As  $\Delta t \rightarrow 0$ ,

$$W_1(\mathcal{K}_{\Delta t}(f^{(k)}), \mathcal{S}_{\Delta t}(f^{(k)})) \leq O\left(\frac{\Delta t^2}{\varepsilon^2}\right). \quad (32)$$

*Proof.* We use the inequality (19) from the first definition of the  $W_1$  distance, which involves the position of particles. Consider two particles that start from the same initial position but evolve under the kinetic and the KDMC simulations, respectively. Let  $x^k$  denote the terminal position of the particles in the kinetic simulation and  $x^{kd}$  denote that in the KDMC simulation. Within one time step of size  $\Delta t$ , two situations are possible:

- **Neither particles collide in the time step.** In this case, both simulations have the same initial states and the same flight time  $\Delta t$ , so the final positions are the same. Thus, no difference between them, so

$$W_1(\mathcal{K}_{\Delta t}(f^{(k)}), \mathcal{S}_{\Delta t}(f^{(k)})) = 0.$$

The probability of a single particle not colliding in  $\Delta t$  is  $e^{-R\Delta t} = 1 - R\Delta t + O(\Delta t^2)$  when  $\Delta t \rightarrow 0$ . Then the probability for this case is  $e^{-R\Delta t}e^{-R\Delta t} = 1 - O(R\Delta t) = 1 - O(\Delta t/\varepsilon^2)$ .

- **At least one particle collides in the time step.** In this case, the distance  $|x^k - x^{kd}|$  is bounded by  $O(\Delta t)$  since the flight time of both particles is less than or equal to  $\Delta t$ . The boundedness holds for all particles following the initial distribution  $f^{(k)}$ . Thus, applying the kinetic and the KDMC simulation on  $f^{(k)}$ , we have

$$W_1(\mathcal{K}_{\Delta t}(f^{(k)}), \mathcal{S}_{\Delta t}(f^{(k)})) \leq O(\Delta t).$$

The probability for this case is  $1 - e^{-R\Delta t}e^{-R\Delta t} = O(\Delta t/\varepsilon^2)$ ,

The weighted sum of these two cases gives the local error

$$W_1(\mathcal{K}_{\Delta t}(f^{(k)}), \mathcal{S}_{\Delta t}(f^{(k)})) \leq O\left(\frac{\Delta t^2}{\varepsilon^2}\right). \quad \square$$

### 3.2.3. KDMC simulation error

Before concluding the analysis of the KDMC simulation error, we briefly comment on the statistical error, which was omitted in the proof of the global error in Section 3.2.1. When simulating in practice, a finite number of samples is used, leading to the statistical error of  $\sigma/\sqrt{N}$  [26], where  $\sigma$  is the standard deviation of the underlying distribution, and  $N$  is the number of samples. This section (Section 3), which concerns the simulation part, mainly focuses on the deterministic errors (also called the bias), e.g., (30) and (32), and the statistical error is assumed to be low in both the KDMC simulation and the reference kinetic simulation, since we can always use more particles to reduce this error. For simplicity, this error is denoted as  $\eta_s = O(1/\sqrt{N})$ . We refer to [32, 33] for the detailed discussion of the statistical error in MC simulation.

Next, the following theorem presents the main error bound for the KDMC simulation.

**Theorem 3.4.** *Let  $f(t^{(k+1)})$  be the reference distribution obtained from the kinetic simulation at time  $t^{(k+1)} = (k+1)\Delta t$  and its approximation obtained from KDMC be  $f^{(k+1)}$ . The error of the KDMC simulation compared with the kinetic simulation, which is the  $W_1$  distance between  $f(t^{(k+1)})$  and  $f^{(k+1)}$ , written as  $\epsilon_s$ , reads*

$$\epsilon_s = W_1(f(t^{(k+1)}), f^{(k+1)}) \leq \eta_s + \begin{cases} O\left(\frac{\varepsilon^2}{\Delta t}\right), & \text{if } \Delta t \gg \varepsilon^2, \\ O\left(\frac{\Delta t}{\varepsilon^2}\right), & \text{if } \Delta t \ll \varepsilon^2, \end{cases} \quad (33)$$

where  $\eta_s = O(1/\sqrt{N})$  is the statistical error.

*Proof.* Recursively substituting the local error (30) into (28), the  $W_1$  distance between the two simulations at time  $t^{(n+1)}$  is

$$W_1(f(t^{(k+1)}), f^{(k+1)}) \leq W_1(f(t^{(k)}), f^{(k)}) + O(\varepsilon^2) \leq O\left(\frac{\varepsilon^2}{\Delta t} t^{(k+1)}\right) = O\left(\frac{\varepsilon^2}{\Delta t}\right), \quad (34)$$

as  $\varepsilon \rightarrow 0$ , given that the initial error  $W_1(f(t^{(0)}), f^{(0)})$  is zero. Therefore, by fixing the time step  $\Delta t$ , the global error (34) of the KDMC simulation is  $O(\varepsilon^2)$ . Similarly, substituting the local error (32) into (28), as  $\Delta t \rightarrow 0$ ,

$$W_1(f(t^{(k+1)}), f^{(k+1)}) \leq O\left(\frac{\Delta t}{\varepsilon^2}\right), \quad (35)$$

which means the global error (35) is  $O(\Delta t)$ . Finally, the combination of (34) and (35) leads to (33), where the two limits  $\varepsilon \rightarrow 0$  and  $\Delta t \rightarrow 0$  are replaced by  $\Delta t \gg \varepsilon^2$  and  $\Delta t \ll \varepsilon^2$ , respectively, under the assumption that  $\Delta t$  and  $\varepsilon$  are both small, for emphasizing the relation between  $\varepsilon$  and  $\Delta t$ . The statistical error  $\eta$  in (33) is due to the finite number of samples in the simulation, and its linear contribution to the total error is justified by the linearity of (1).  $\square$

The error (33) is between the distributions simulated from the kinetic simulation and the KDMC simulation at a time  $t = (k+1)\Delta t$ , which corresponds to the time-terminal simulation in Appendix A. If the time-integrated simulation is applied, which accumulates the distribution at all times  $t_l = l\Delta t$  with  $l = 1, 2, \dots, k$ , a smaller error is typically observed. This fact can be seen as follows.

The normalized time-integrated distributions of  $f(t^{(k)})$  and  $f^{(k)}$  at the time  $t^{(k)}$  are

$$\frac{\sum_{l=1}^k f(t^{(l)})}{\int_{\Omega} \sum_{l=1}^k f(t^{(l)}) dx} = \frac{\sum_{l=1}^k f(t^{(l)})}{k \int_{\Omega} f(t^{(0)}) dx}, \quad \text{and} \quad \frac{\sum_{l=1}^k f^{(l)}}{\int_{\Omega} \sum_{l=1}^k f^{(l)} dx} = \frac{\sum_{l=1}^k f^{(l)}}{k \int_{\Omega} f^{(0)} dx}, \quad (36)$$

where  $\Omega$  is the spatial domain of the distributions, and the equalities are due to the mass-conservation as explained in Section 3.1. We also have the equality of the initial mass  $\int_{\Omega} f(t^{(0)}) dx = \int_{\Omega} f^{(0)} dx$  since the initial condition is the same. Then, the  $W_1$  distance between the two time-integrated simulations is

$$W_1\left(\frac{1}{k} \sum_{l=1}^k f(t^{(l)}), \frac{1}{k} \sum_{l=1}^k f^{(l)}\right) \leq \frac{1}{k} \sum_{l=1}^k W_1(f(t^{(l)}), f^{(l)}) \leq W_1(f(t^{(k)}), f^{(k)}), \quad (37)$$

where the first inequality is due to the convexity of the  $W_1$  metric [30], and the last quantity is  $\epsilon_s$  in (33). The normalization factors  $\int_{\Omega} f(t^{(0)}) dx$  and  $\int_{\Omega} f^{(0)} dx$  are not written explicitly as stated in Remark 1.

## 4. Estimation error

KDMC is a hybrid approach that consists of kinetic and diffusive simulations. In this work, the standard MC estimator (15) is used to score, i.e., to compute, the moments of the kinetic part, and the fluid estimation, derived in Section 2.4, is used to score the moments of the diffusive part. The overall estimation error is the combination of errors in these two estimation parts. To analyze the estimation error, we decompose it into the kinetic and diffusive parts in Section 4.1, which are then analyzed separately in Sections 4.2 and 4.3, respectively.

The reference solution is computed by the standard MC method, which simulates particle trajectories as in Section 2.3.1 and estimates the moment using the standard MC estimator (15). For brevity, we refer to this method as the kinetic method. The KDMC simulation introduced in Section 2.3 together with the associated fluid estimation described in Section 2.4 is referred to as the KDMC method or simply KDMC. The moments (3) are smooth functions, so we choose the relative  $L_2$  norm to measure errors.

### 4.1. Estimation error decomposition

We denote the reference moment obtained from the kinetic method by  $m^k$ , and the approximate moment obtained from KDMC by  $m^{kd}$ , which includes the kinetic component  $m^{kd,k}$  and the diffusive component  $m^{kd,d}$ , that is,  $m^{kd} = m^{kd,k} + m^{kd,d}$ . Let  $\alpha \in [0, 1]$  denote the expected fraction of the duration of the kinetic step within a time step of size  $\Delta t$ . In a homogeneous background, where the collision rate  $R(x) = R$  is constant, the coefficient  $\alpha$  remains constant within each time step  $\Delta t$  and thus throughout the entire simulation. Under the  $L_2$  norm, the relative estimation error is

$$\epsilon_{kd} = \|m^k - m^{kd}\|_2 / \|m^k\|_2 = \|\alpha m^k - m^{kd,k} + (1 - \alpha)m^k - m^{kd,d}\|_2 / \|m^k\|_2 \leq \alpha \epsilon_k + (1 - \alpha) \epsilon_{kd}, \quad (38)$$

where  $m^{kd} = m^{kd,k} + m^{kd,d}$  is substituted in, and

$$\epsilon_k = \|\alpha m^k - m^{kd,k}\|_2 / (\alpha \|m^k\|_2), \quad \text{and} \quad \epsilon_d = \|(1 - \alpha)m^k - m^{kd,d}\|_2 / ((1 - \alpha) \|m^k\|_2), \quad (39)$$

are defined as the relative kinetic and diffusive estimation errors, and discussed in Sections 4.2 and 4.3, respectively. Intuitively, the moment from the kinetic part  $m^{kd,k}$  contributes an  $\alpha$  portion of the approximate moment  $m^{kd}$  and its error should therefore be measured relative to the corresponding portion of the reference moment,  $\alpha m^k$ . The same interpretation holds for the diffusive part and its corresponding relative error  $\epsilon_d$ .

To derive the coefficient  $\alpha$ , let  $\tau \sim \text{Exp}(R)$  be the kinetic flight time of a particle in a time step  $\Delta t$ . The particle flies for time  $\tau$  if  $\tau < \Delta t$ ; otherwise, it flies for  $\Delta t$ . So the expectation is the weighted sum of these two events, i.e.,

$$\mathbb{E}[\tau] = \int_0^{\Delta t} \tau R e^{-R\tau} d\tau + \Delta t e^{-R\Delta t} = (1 - e^{-R\Delta t}) / R,$$

where  $e^{-R\Delta t}$  is the probability that the particle does not collide in  $\Delta t$ . Then the coefficient

$$\alpha = \mathbb{E}[\tau] / \Delta t = (1 - e^{-R\Delta t}) / R\Delta t. \quad (40)$$

Since  $R\Delta t \in (0, \infty)$ , we have limits

$$\lim_{R\Delta t \rightarrow 0} \alpha = 1, \quad \text{and} \quad \lim_{R\Delta t \rightarrow \infty} \alpha = 0.$$

From  $R\Delta t = 0$  to  $\infty$ , the coefficient  $\alpha$  monotonically decreases from 1 to 0. In practice, we assume  $R = O(1/\varepsilon^2) \gg 1$  and  $\Delta t \ll 1$ . Then, we can conclude from (38) that

- If  $\Delta t \gg \varepsilon^2$ , that is  $\varepsilon \rightarrow 0$ , then  $\alpha \rightarrow 0$  and the diffusive part  $m^{kd,d}$  dominates the estimated moment  $m^{kd}$ .
- If  $\Delta t \ll \varepsilon^2$ , that is  $\Delta t \rightarrow 0$ , then  $\alpha \rightarrow 1$  and the kinetic part  $m^{kd,k}$  dominates the estimated moment  $m^{kd}$ .

Hence, the estimation error (38) can be approximated as

$$\epsilon_{kd} \approx \begin{cases} \epsilon_d, & \text{if } \Delta t \gg \varepsilon^2, \\ \epsilon_k, & \text{if } \Delta t \ll \varepsilon^2. \end{cases} \quad (41)$$

This formula (41) is based on the homogeneous background assumption, that is, we assume  $R(x) = R$  is constant. In fact, for a moderate heterogeneous background, this formula still holds. By moderate, we refer to cases where  $R(x) = r(x)/\varepsilon^2$ , and the range of the function  $r(x)$  is bounded such that  $R(x) = O(1/\varepsilon^2)$ , which is also the assumption of the fluid limit in Section 2.2. Under the moderate assumption, the diffusive step remains dominant in each time step of size  $\Delta t$ , and thus  $\epsilon_{kd} = \epsilon_d$  if  $\Delta t \gg \varepsilon^2$ ; the reverse holds when  $\Delta t \ll \varepsilon^2$ . In Section 5.6, we numerically show that (41) holds for the moderate heterogeneous background with a fusion-relevant test case. Next, we discuss  $\epsilon_k$  and  $\epsilon_d$  separately, and subsequently combine them to derive the expression in (41).

#### 4.2. Error of kinetic part $\epsilon_k$

We discuss the kinetic error in two limiting cases:  $\Delta t \rightarrow 0$  and  $\varepsilon \rightarrow 0$ . In the kinetic part, the moments  $m^{kd,k}$  defined in Section 4.1 are scored by the unbiased MC estimator (15). Thus, the error is purely statistical.

##### 4.2.1. Error of kinetic part as $\Delta t \rightarrow 0$

As explained in Section 3.2.3, the statistical error is  $\sigma/\sqrt{N}$  with the standard deviation  $\sigma$  and the number of samples  $N$ . In each time step  $\Delta t$ , one and only one kinetic flight happens. If the total number of particles  $I$  is fixed, more segments result in more samples for the estimator. Thus, the error is then lower. In particular, the number of time steps is  $K = \bar{t}/\Delta t$  where  $\bar{t}$  is the simulation time, and the total number of samples  $N$  used in the MC estimator is  $N = KI$ . Thus, the error scales as  $\sigma/\sqrt{KI} = \sigma\sqrt{\Delta t}/\sqrt{I} = O(\sqrt{\Delta t})$  if  $\sigma$  and  $I$  are fixed.

However, this error cannot vanish entirely. For instance, if a collision-based estimator is used, where only collisions contribute to the estimate. The probability that a particle does not collide in a time step  $\Delta t$  is  $e^{-R\Delta t}$  with  $R = O(1/\varepsilon^2)$ . Thus, the particle is not likely to collide in the time step, when  $\Delta t \ll \varepsilon^2$ . Further reducing  $\Delta t$  does not reduce this statistical error. If a track-length estimator is used, which scores the flight distance instead of the collision, successive samples become highly correlated when  $\Delta t \ll \varepsilon^2$ . The effective number of independent samples no longer scales with the number of time steps. Therefore, the statistical error stagnates. So, if denoting the stagnated error as  $\eta_k$ , we have

$$\epsilon_k = \eta_k, \quad \text{if } \Delta t \ll \varepsilon^2, \quad (42)$$

where  $\eta_k = O(1/\sqrt{I})$  since  $\Delta t$  has no effect on the statistical error if  $\Delta t \ll \varepsilon^2$ , as explained above. The error of the kinetic part dominates only if  $\Delta t \ll \varepsilon^2$  as shown in (41), and thus the case  $\epsilon_k = O(\sqrt{\Delta t})$  if  $\Delta t \gg \varepsilon^2$  is not important.

##### 4.2.2. Error of kinetic part as $\varepsilon \rightarrow 0$

We assume the time step  $\Delta t$  and the number of particles  $I$  are fixed, and start from the collision rate being small. When  $\varepsilon \rightarrow \infty$ , the collision rate  $R = O(1/\varepsilon^2) \rightarrow 0$ , and no collisions happen. As a result, in both the kinetic and the KDMC simulations, particles fly with the initial velocity over the whole simulation time  $\bar{t}$ , which causes no difference between the moments estimated by the two methods.

As  $\varepsilon$  decreases, the number of collisions  $R\bar{t} = O(1/\varepsilon^2)$  increases, with  $\bar{t}$  the simulation time. These collisions lead to different trajectories for the two simulations, and this difference introduces statistical fluctuations, which contribute to the variance of the MC estimator. The variance  $\sigma^2$  is then proportional to the number of collisions, and thus to  $O(1/\varepsilon^2)$ . The statistical error  $\sigma/\sqrt{N}$  is then  $O(1/(\varepsilon\sqrt{N})) = O(1/\varepsilon)$  as  $N = KI$  is fixed. When  $\Delta t \gg \varepsilon^2$ , particles are likely to collide in each  $\Delta t$ . The variance, and therefore the statistical error, stagnates. The error of the kinetic part dominates only when  $\Delta t \ll \varepsilon^2$  as illustrated in (41), and thus it is not need to discuss the error of the kinetic part when  $\Delta t \gg \varepsilon^2$ . Finally, the error of the kinetic part is small when  $\varepsilon$  is large, then it increases as  $O(1/\varepsilon)$  when  $\Delta t \ll \varepsilon^2$ . Thus, we have

$$\epsilon_k = O\left(\frac{1}{\varepsilon}\right), \quad \text{if } \Delta t \ll \varepsilon^2. \quad (43)$$

We remark that the  $\Delta t$  affects the statistical error by changing the number of samples, and the diffusive scaling parameter  $\varepsilon$  affects the statistical error by changing the variance  $\sigma^2$ . In both limit cases, the statistical error starts to stagnate around  $\Delta t = \varepsilon^2$ . Thus, the two stagnation errors are expected to be of comparable magnitude.

In fact, the variance of the kinetic part is also affected by the mean plasma velocity  $u_p$ , especially for the  $m_1$  (3). A detailed discussion of  $u_p$  is beyond the scope of this work, but we mention it briefly here. The MC estimator (15), like the track-length and collision estimator [22], involves the sampling of  $v^l$  with the particle velocity  $v$  following the

normal distribution  $N(u_p, \sigma_p^2)$  and  $l = 0, 1, 2$ . When  $l$  is odd, the value  $v^l$  fluctuates around zero, especially when the mean  $u_p$  is small. In this case, the summation of negative and positive samples in the estimator (15) may cancel each other out, causing a large variance. However, this is not the case if  $l$  is even, since  $v^l$  would always be positive. A rigorous proof can be done by writing down the expression of the variance for the sample  $v^l$ . We leave the proof for future work and conclude that if the MC estimation (15) is used, the  $m_1$  moment has a greater variance than the  $m_0$  and  $m_2$  moments when  $u_p$  is small. This fact is shown numerically in Section 5.3.

#### 4.3. Error of diffusive part $\epsilon_d$

The diffusive part estimation consists of multiple error components. We first analyze each error and subsequently explain how these errors combine to form the overall error of the diffusive part.

##### 4.3.1. Propagated error from KDMC simulation $\epsilon_i$

The fluid estimation scores moments by solving the fluid model (4) with the initial condition  $\hat{\rho}_0(x)$  provided by KDMC as shown in (16). However, this initial condition is not the exact initial particle distribution since the KDMC simulation introduces an error  $\epsilon_s$  as shown in (33). This initial error propagates through the fluid model solution. Below, we show that the resulting propagated error, denoted as  $\epsilon_i$ , has the same asymptotic bound as  $\epsilon_s$ .

Let the true initial distribution be  $\rho_0(x)$  and the corresponding true solution of the fluid model be  $\rho(x, t)$ . Similarly, let the solution given by the inexact initial condition  $\hat{\rho}_0(x)$  be  $\hat{\rho}(x, t)$ . Rewrite the fluid model (4) in the operator form

$$\partial_t \rho(x, t) = \mathcal{L} \rho(x, t), \quad (44)$$

where  $\mathcal{L}$  is the linear spatial operator in (4). Since this model is linear, its solution can be expressed as

$$\rho(x, t) = e^{-\mathcal{L}t} \rho(x, t=0). \quad (45)$$

The propagated error in the solution at time  $t$  is then given by

$$\epsilon_i = \|\rho(x, t) - \hat{\rho}(x, t)\|_2 = \|e^{-\mathcal{L}t} (\rho_0(x) - \hat{\rho}_0(x))\|_2 \leq e^{-ct} \|\rho_0(x) - \hat{\rho}_0(x)\|_2, \quad (46)$$

where  $c$  is a constant. The term  $\|\rho_0(x) - \hat{\rho}_0(x)\|_2$  is the difference of the initial conditions under the  $L_2$  norm, which is the KDMC error  $\epsilon_s$  described in (33). Since  $e^{-ct}$  in (46) is independent of  $\epsilon$  and  $\Delta t$ , the propagated error  $\epsilon_i$  has the same convergence as  $\epsilon_s$  with respect to  $\epsilon$  and  $\Delta t$ . Therefore,

$$\epsilon_i = \eta_s + \begin{cases} \mathcal{O}\left(\frac{\epsilon^2}{\Delta t}\right), & \text{if } \Delta t \gg \epsilon^2, \\ \mathcal{O}\left(\frac{\Delta t}{\epsilon^2}\right), & \text{if } \Delta t \ll \epsilon^2, \end{cases} \quad (47)$$

where  $\eta_s$  is a statistical error that we assume to be negligible.

**Remark 2** (Errors with different norms). *The WS distance and the  $L_2$  norm measure fundamentally different error aspects. The former measures the "effort" to transport one distribution to another, and has units of distance. The latter measures the energy (squared difference) between vectors, and has units of the square of the quantity being measured. Thus, it is nontrivial to mix them when computing precise quantities. Nevertheless, we observe numerically that the simulation error  $\epsilon_s$  in the  $L_2$  norm exhibits the same convergence rate as in the  $W_1$  distance.*

##### 4.3.2. Model error in the moment calculation $\epsilon_m$

After solving the fluid model (4), the moments of the diffusive part are calculated as (5)-(7). We now show that the error in these moment calculations is bounded by  $\mathcal{O}(\epsilon^2)$ . According to the derivation of the fluid model in Section 2.2, we know

$$\|f(x, v, t) - f_f(x, v, t)\|_2 = \|\epsilon^2 f_2(x, v, t) + \epsilon^3 f_3(x, v, t) + \dots\|_2 = \mathcal{O}(\epsilon^2). \quad (48)$$

Here we use the fact that  $f_2(x, v, t)$  is bounded by a constant independent of  $\epsilon$  [6]. A rigorous proof of (48) can be found in [5]. Further, we bound the error of moments (3) as

$$\epsilon_m = \left\| \int_{-\infty}^{\infty} v^l f(x, v, t) - v^l f_f(x, v, t) dv \right\|_2 \leq \int_{-\infty}^{\infty} \|v^l\|_2 \|f(x, v, t) - f_f(x, v, t)\|_2 dv \leq \mathcal{O}(\epsilon^2) \int_{-\infty}^{\infty} \|v^l\|_2 dv = \mathcal{O}(\epsilon^2), \quad (49)$$

with  $l = 0, 1, 2$  corresponding to, respectively,  $m_0(x)$ ,  $m_1(x)$  and  $m_2(x)$  in (5)-(7).

#### 4.3.3. Time evolution error $\epsilon_{\Delta t}$

In the fluid estimation procedure, we use the average duration of all diffusive steps for the evolution time of the fluid model (4), as explained in Section 2.4. Since the time of each diffusive step is less than  $\Delta t$ , the error for the averaging is bounded by  $O(\Delta t)$ . In addition, the averaging (17) is empirical, leading to an additional statistical error. Thus, the simulation time of the fluid model (4) has the error

$$\delta_{\Delta t} = O(\Delta t) + \eta_{\Delta t}, \quad (50)$$

where  $\eta_{\Delta t} = O(1/\sqrt{N})$  is the statistical error, which is assumed to be negligible, due to the limited number of diffusive steps, as discussed in Section 3.2.3.

The biased simulation time (50) affects the solution of the fluid model as follows. Let  $\rho(x, t)$  be the true solution of fluid model (4) at time  $t$ , and  $\rho(x, t + \delta_{\Delta t})$  is the solution simulated with the biased simulation time. Given the first-order Taylor expansion of  $\rho(x, t + \delta_{\Delta t})$

$$\rho(x, t + \delta_{\Delta t}) = \rho(x, t) + \delta_{\Delta t} \partial_t \rho(x, t) + O(\delta_{\Delta t}^2), \quad (51)$$

the error due to the biased simulation time, which refers to the time evolution error, is then

$$\epsilon_{\Delta t} = \|\rho(x, t + \delta_{\Delta t}) - \rho(x, t)\|_2 = \|\delta_{\Delta t} \partial_t \rho(x, t) + O(\delta_{\Delta t}^2)\|_2 = \|\delta_{\Delta t}\|_2 = O(\Delta t) + \eta_{\Delta t}, \quad (52)$$

where  $\partial_t \rho(x, t)$  is independent of  $\Delta t$  and  $\eta_{\Delta t}$ . For a homogeneous background, the averaging provides an unbiased estimate of the true evolution time since each diffusive time follows the same distribution  $\text{Exp}(R)$  when  $R(x) = R$ , that is, all samples are independent and identically distributed. As a result, only a small statistical error is introduced.

#### 4.3.4. Discretization errors $\epsilon_x$ and $\epsilon_t$

Last, the numerical solution of the fluid model (4) introduces spatial and temporal discretization errors, denoted as  $\epsilon_x$  and  $\epsilon_t$ , respectively. In this work, we use an upwind scheme for the advection term and a central difference scheme for the diffusive term, resulting in first-order accuracy in both space and time. Consequently, the spatial discretization error  $\epsilon_x = O(\Delta x)$  with  $\Delta x$  the spatial step size. As the evolution time of this equation in the fluid estimation procedure is less than  $\Delta t$ , the time step used in the numerical solver will be much smaller than  $\Delta t$ . This ensures  $\epsilon_t$  is  $O(\Delta t)$ . In practice,  $\epsilon_t$  is negligible compared to  $\epsilon_{\Delta t} = \eta_{\Delta t} + O(\Delta t)$ , and we omit it from further discussion.

It is trivial to prove that the error of the fluid estimation is the sum of the above-listed errors, due to the linearity of the Boltzmann-BGK equation (1) and the fluid model (4). Therefore, we skip the proof and have

$$\epsilon_d = \epsilon_m + \epsilon_{\Delta t} + \epsilon_x + \epsilon_t = O(\varepsilon^2) + O(\Delta t) + O(\Delta x) + \eta + \begin{cases} O\left(\frac{\varepsilon^2}{\Delta t}\right), & \text{if } \Delta t \gg \varepsilon^2, \\ O\left(\frac{\Delta t}{\varepsilon^2}\right), & \text{if } \Delta t \ll \varepsilon^2. \end{cases} \quad (53)$$

where  $\eta = \max(\eta_s, \eta_k, \eta_{\Delta t}) = O(1/\sqrt{N})$  is the statistical error, assumed to be small.

We conclude our discussion of the simulation error by neglecting the discretization error and the influence of the number of particles  $I$ , as our focus is on the performance of the KDMC method with respect to the time step  $\Delta t$  and the diffusive scaling parameter  $\varepsilon$ . Next, we substitute the error bound for the kinetic part (42), (43), and that for diffusive part (53) into the error formula (41), we obtain

$$\epsilon_{kd}(\varepsilon) = \begin{cases} O\left(\frac{\varepsilon^2}{\Delta t}\right), & \text{if } \Delta t \gg \varepsilon^2, \\ O\left(\frac{1}{\varepsilon}\right), & \text{if } \Delta t \ll \varepsilon^2, \end{cases} \quad \text{and} \quad \epsilon_{kd}(\Delta t) = \begin{cases} O\left(\frac{1}{\Delta t}\right), & \text{if } \Delta t \gg \varepsilon^2, \\ O(\Delta t), & \text{if } \Delta t \ll \varepsilon^2, \end{cases} \quad (54)$$

where  $\epsilon_{kd}(\varepsilon)$  denotes the estimation error when the time step  $\Delta t$  is fixed and the error depends only on the diffusive scaling parameter  $\varepsilon$ , whereas  $\epsilon_{kd}(\Delta t)$  denotes the error when  $\varepsilon$  is fixed and the error depends only on  $\Delta t$ . Note that, when  $\Delta t \ll \varepsilon^2$ , the kinetic part error  $\eta$  in (42) is expected to dominate  $\epsilon_{kd}(\Delta t)$ . However, since  $\eta_k$  is assumed small, the diffusive part error, which is of order  $O(\Delta t)$ , remains significant. Consequently, we have  $\epsilon_{kd}(\Delta t) = O(\Delta t)$  if  $\Delta t \ll \varepsilon^2$ .

## 5. Numerical experiments

This section numerically validates the theoretical analysis presented in Sections 3 and 4. The convergence of the KDMC simulation is examined in Section 5.1. For the estimation procedure, we introduce a test case in Section 5.2, with which the estimation errors of the kinetic and diffusive parts are then displayed separately in Sections 5.3 and 5.4, respectively. The total estimation error is presented in Section 5.5. All experiments in Section 5.1- 5.4 make use of a homogeneous background. To illustrate the effectiveness of KDMC and our analysis in a more realistic context, a heterogeneous fusion-relevant test case is presented in Section 5.6. Finally, the computational cost of KDMC is analyzed in Section 5.7. Throughout this work, we specify the key parameters necessary to interpret our results and refer to our code repository [34] for further details.

### 5.1. KDMC simulation error

In Section 3, we proved the local error bounds for the KDMC simulation with respect to the diffusive scaling parameter  $\varepsilon$  (30) and the time step  $\Delta t$  (32), along with the global error bound (33) under the  $W_1$  distance metric.

In numerical experiments, we use the kinetic simulation described in Section 2.3.1 as a reference solution, and compare the particle distributions from the kinetic and the KDMC simulation at a terminal time  $\bar{t}$ . All particles start from the initial position  $x_0 = 0$  and the initial velocity  $v_0$  following the Maxwellian distribution (2). The collision rate  $R$  and the variance  $\sigma_p^2$  are both equal to  $1/\varepsilon^2$  with the diffusive scaling parameter  $\varepsilon \in [10^{-3}, 10^0]$ , the mean velocity is  $u_p = 2$ , and the time step is  $\Delta t = \bar{t}/K$  with  $K \in [10^0, 10^4]$ .

The local error is the error made in a single time step. That is, in both the kinetic and KDMC simulations, particles evolve up to time  $\Delta t$ . The local error is obtained by calculating the  $W_1$  distance (20) between the two resulting distributions at  $\Delta t$ . This error is illustrated in Figure 2 with the number of particles  $I = 5 \times 10^7$ . In Figure 2a, we fix  $\Delta t = \bar{t}/5$  and plot the  $W_1$  distance against  $\varepsilon$ . The result shows that the local error scales as  $\mathcal{O}(\varepsilon^2)$  as  $\varepsilon \rightarrow 0$ . When  $\varepsilon = 0.1$  is fixed and the time step varies, as demonstrated in Figure 2b, the error decreases as  $\mathcal{O}(\Delta t^2)$  as  $\Delta t \rightarrow 0$ . These observations are consistent with the analytical order of the local errors (30) and (32), respectively.

To evaluate the global error, we let  $10^7$  particles evolve up to the terminal time  $\bar{t} = 0.0275$  instead of performing just a single time step  $\Delta t$ . The convergence is illustrated in Figure 3. For fixed  $\Delta t$ , Figures 3a and 3b show the global error decreases as  $\mathcal{O}(\varepsilon^2)$  when  $\Delta t \gg \varepsilon^2$  and increases as  $\mathcal{O}(1/\varepsilon^2)$  when  $\Delta t \ll \varepsilon^2$ . The largest bias of the KDMC simulation is around  $\Delta t = \varepsilon^2$  given the form of the error bound (33). Similarly, for fixed  $\varepsilon$ , Figures 3c and 3d demonstrate that the global error decreases as  $\mathcal{O}(\Delta t)$  when  $\Delta t \ll \varepsilon^2$  and grows like  $\mathcal{O}(1/\Delta t)$  when  $\Delta t \gg \varepsilon^2$ . In some cases, such as around  $\Delta t = 10^{-5}$  in Figure 3c, the observed decay is faster than  $\mathcal{O}(\Delta t)$ , indicating that the bound in (33) is not always sharp. Nevertheless, the simulation results generally align well with the theoretical prediction. In Section 4, we showed that there are other error terms bounded by  $\mathcal{O}(\varepsilon^2)$  and  $\mathcal{O}(\Delta t)$  in the bound of the total estimation error (54). Thus, there is no need to further sharpen the error bound.

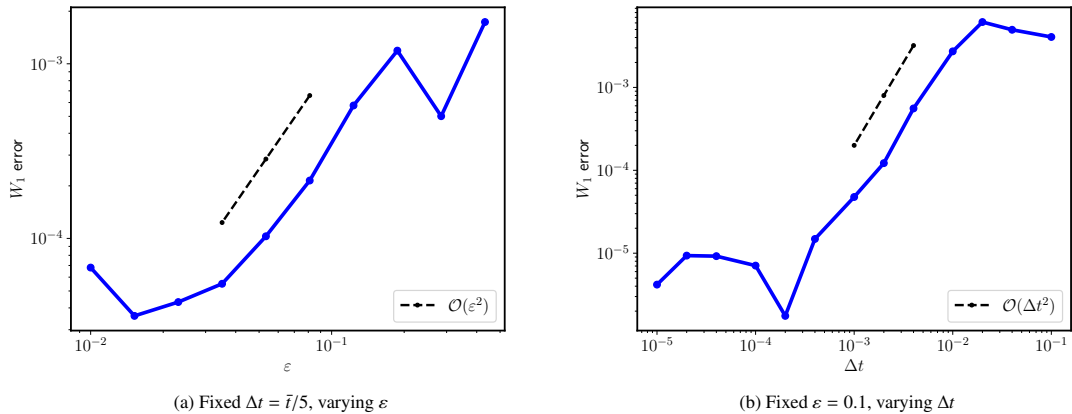


Figure 2: Local KDMC simulation error. Left: fixed  $\Delta t$ , the error decreases as  $\mathcal{O}(\varepsilon^2)$ . Right: fixed  $\varepsilon$ , the error decreases as  $\mathcal{O}(\Delta t^2)$ .

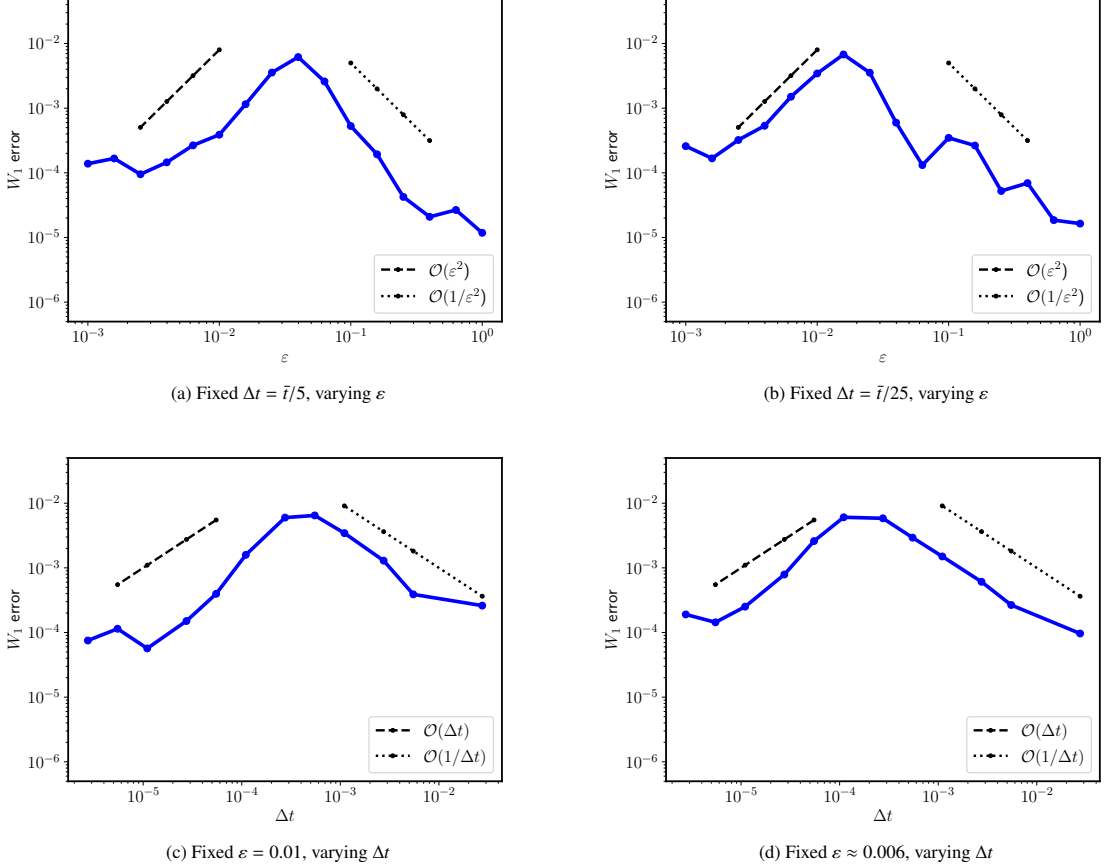


Figure 3: Global KDMC simulation error. First row: convergence with fixed  $\Delta t$ . Second row: convergence with fixed  $\varepsilon$ .

### 5.2. Homogeneous test case for estimation

In this test case, the particle system, defined over the periodic domain  $x \in [0, 1]$ , evolves over the time interval  $t \in [0, \bar{t}]$  with  $\bar{t} = 0.0275$ . The variance of the plasma velocity and the collision rate are

$$\sigma_p^2(x) = \frac{1}{\varepsilon^2}, \quad \text{and} \quad R(x) = \frac{1}{\varepsilon^2}, \quad (55)$$

respectively. The mean velocity is  $u_p = 30$  unless stated otherwise. The parameter  $\varepsilon$  ranges from 0.01 to 1, implying a maximum collision rate of  $10^4$ . As the initial condition, particles have position  $x_0$  sampled from the density

$$\rho(x, t = 0) = 1 + \frac{1}{2\pi} \sin(2\pi x), \quad x \in [0, 1], \quad (56)$$

and velocities following the Maxwellian distribution  $M(v|x_0)$  given by (2). A periodic boundary condition is imposed on the spatial domain.

In the numerical experiments, the three moments (3) are discretized spatially as mentioned in Section 2.4. If the reference moments are  $m_l = [m_{l,1}, \dots, m_{l,J}]$ , and the approximate moments are  $\hat{m}_l = [\hat{m}_{l,1}, \dots, \hat{m}_{l,J}]$ , with  $l = 0, 1, 2$ , the relative  $L_2$  error  $E$  with respect to the reference moments is thus calculated as

$$E = \frac{\left( \sum_{j=1}^J (m_{l,j} - \hat{m}_{l,j})^2 \right)^{1/2}}{\left( \sum_{j=1}^J m_{l,j}^2 \right)^{1/2}}. \quad (57)$$

### 5.3. Estimation error: kinetic part

We now present the numerical results for the estimation errors under the relative  $L_2$  metric (57), starting with the error in the kinetic part as defined in (39). To calculate the error (39), we first need to isolate the kinetic part of the estimated moment  $m^{kd,k}$  from the total moment  $m^{kd}$  and construct the reference solution  $am^k$ .

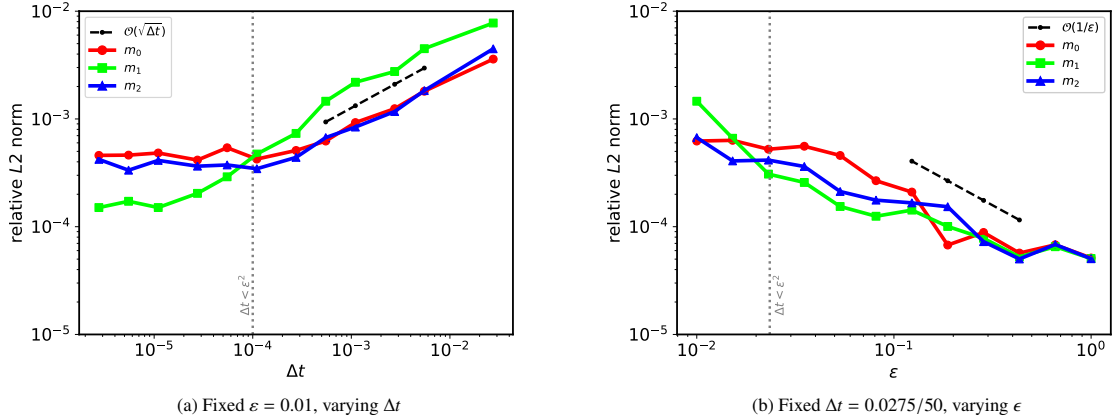


Figure 4: Kinetic part estimation error with  $u_p = 30$ .

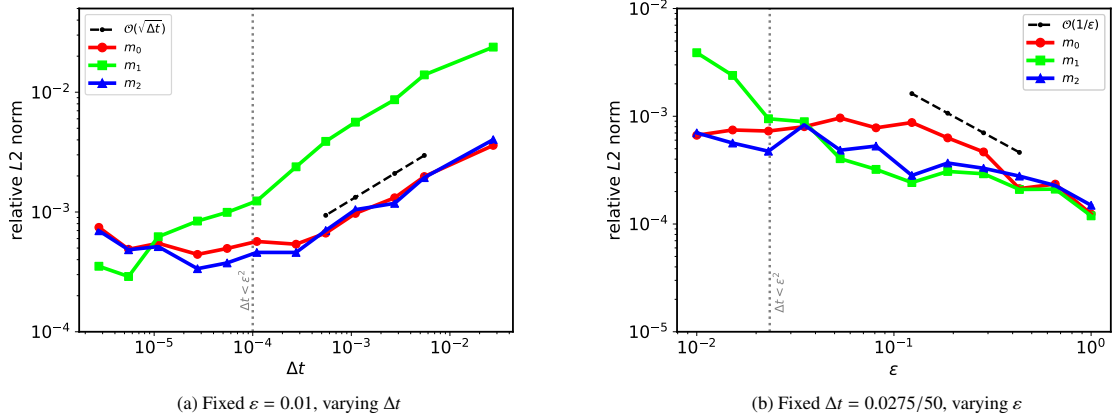


Figure 5: Kinetic part estimation error with  $u_p = 10$ . A smaller  $u_p$  leads to a larger error of the  $m_1$  moment

Due to the hybrid procedure of kinetic and diffusion motions in KDMC, isolating the kinetic part is not straightforward, since the  $k$ -th kinetic step is inherently influenced by the  $i = 0, \dots, k-1$ -th diffusive steps. To address this and obtain the approximate moment  $m^{kd,k}$ , we let the diffusive steps be mimicked using kinetic motions that we do not score. Specifically, within each  $\Delta t$  time segment, the first kinetic step is scored by the MC estimator (15). Instead of a diffusive step (11), particles move kinetically as (8) for the rest of the time without scoring. In this way, the simulation only has a negligible statistical error, and the estimation error of the diffusive part is removed, as the kinetic motion is unbiased and no diffusive motion exists. (Note that forcing particles to stop at  $\Delta t$  with kinetic steps is unbiased, thanks to the memorylessness property of the exponential distribution for sampling the free-flight time  $\tau$  used in Section 2.3.1.) The reference moment  $am^k$  is obtained by repeating the above process with different random seeds, since the kinetic simulation is used throughout, and scoring only the kinetic part (the first step within a time step) recovers the reference  $am^k$ . The error of the kinetic part is then calculated by comparing  $m^{kd,k}$  and  $m^k$  under the relative  $L_2$  metric (57).

Figure 4 shows the kinetic error obtained in this manner with  $10^7$  particles in both experiments for the reference and approximation. In all figures that follow, red, green, and blue represent the error of the moments  $m_0$ ,  $m_1$ , and  $m_2$ ,

respectively. The vertical dashed line indicates the point  $\Delta t = \varepsilon^2$  where the error is expected to stagnate. Figure 4a presents the relative  $L_2$  error against the time step  $\Delta t$  with the scaling parameter  $\varepsilon = 0.01$ . The error scales as  $O(\sqrt{\Delta t})$  initially and stagnates when  $\Delta t \ll \varepsilon^2$ . The stagnation starts around  $\Delta t = \varepsilon^2$  as expected. Next, we fix  $\Delta t = \bar{t}/50$  (i.e., 50 time steps) and vary  $\varepsilon$  in Figure 4b. The error grows at the rate  $O(1/\varepsilon)$  as  $\varepsilon$  decreases, and stagnates when  $\Delta t \gg \varepsilon^2$ . The stagnation starts again around  $\Delta t = \varepsilon^2$ . In both cases, the stagnation occurs at roughly the same magnitude as predicted in Section 4.2.2. In total, the results are consistent with the analytical error (42) and (43) in Section 4.2.

As described in Section 4.2, the  $m_1$  moment has a larger error than the  $m_0$  and  $m_2$  moments if  $u_p$  is small. To show this, let  $u_p = 10$  instead of 30, and repeating the experiment above, we get the convergence plot shown in Figure 5. It can be seen that the  $m_0$  and  $m_2$  moments are similar to those shown in Figure 4, but the  $m_1$  moment has a greater error in the regime  $\Delta t \gg \varepsilon^2$ .

#### 5.4. Estimation error: diffusive part

In this section, we study the estimation error of the diffusive part numerically. We first illustrate its components: the model error  $\epsilon_m$ , the spatial discretization error  $\epsilon_x$  in Section 5.4.1 and the time discretization error  $\epsilon_{\Delta t}$  in Section 5.4.2. Subsequently, the estimation error of the diffusive part, including the error propagated from the initial error  $\epsilon_i$ , is illustrated in Section 5.4.3. The corresponding theoretical analysis can be found in Section 4.3. As before, the three colors: red, green, and blue represent the error of the moments  $m_0$ ,  $m_1$ , and  $m_2$ , respectively, in all plots.

##### 5.4.1. Model error $\epsilon_m$ and discretization error $\epsilon_x$

Estimating the moments using the fluid model (4), which approximates the Boltzmann-BGK equation (1), introduces a model error  $\epsilon_m = O(\varepsilon^2)$ . Moreover, the spatial discretization error  $\epsilon_x$  may dominate when the solver of the fluid model is not accurate enough. In the numerical experiments, the approximate moments are estimated as (5)-(7) by solving the fluid model in Section 2.2 via the upwind scheme. To study the effect of spatial discretization, we use two mesh resolutions: 200 and 1000 grid cells. This allows us to observe the discretization error  $\epsilon_x$ . For reference, we take the moments estimated by the kinetic method with  $N = 10^8$  particles and 1000 grid cells. If fewer particles were used, the second-order convergence in space would be obscured by the statistical error in the reference solution.

The numerical results for both grid resolutions are presented in Figure 6. In both cases, we see that when  $\varepsilon$  is large, the fluid model is not an accurate approximation, and the error does not decrease significantly. As  $\varepsilon$  decreases, the expected second-order convergence, i.e.,  $O(\varepsilon^2)$ , becomes evident. However, for 200 cells, the error of  $m_1$  stagnates near  $\varepsilon = 0.01$ , indicating that another error dominates. This dominant error is the discretization error. This fact is confirmed in Figure 6b, where increasing the number of cells to 1000 reduces the error of  $m_1$  by nearly an order of magnitude, and the errors of the other two moments also reduce slightly.

The obvious discretization error in  $m_1$  moment is due to the spatial derivative term in its definition (6). In contrast,  $m_0$  contains no derivative term, making it less sensitive to spatial discretization. Although the  $m_2$  moment (7) does have the derivative term, its non-derivative term has a much greater value when  $\varepsilon$  is small. Consequently, the relative contribution of the discretization error is less significant for  $m_2$ .

##### 5.4.2. Time evolution error $\epsilon_{\Delta t}$

As analyzed in Section 4.3, only a statistical error exists when approximating the evolution time of the fluid estimation by the averaging with a homogeneous background, i.e.,  $\epsilon_{\Delta t} = \eta = O(1/\sqrt{I})$ , where  $I$  is the number of particles. To verify  $\epsilon_{\Delta t} = \eta$  numerically, we first isolate the error of the diffusive part from the total estimation error, and then isolate the time evolution error  $\epsilon_{\Delta t}$  from the error of the diffusive part. In the diffusive part, the error can be decomposed as  $\epsilon_d = \epsilon_m + \epsilon_{\Delta t} + \epsilon_x + \epsilon_i$  (see (53)). Among these, only  $\epsilon_{\Delta t}$  and the propagated error  $\epsilon_i$  depend on the time  $t$ . We then need to remove the propagated error from the KDMC simulation  $\epsilon_i$  for focusing solely on  $\epsilon_{\Delta t}$ . This can be done similarly to the strategy used in Section 5.3, that is, mimicking the diffusive motion with the kinetic motion.

In particular, to construct the reference solution, we fix the time step size  $\Delta t$  in the kinetic method as in the experiment in Section 5.3. In each  $\Delta t$ , the first flight is not scored, but the remaining mimicked diffusive part is scored. As a result, we obtain the moments only contributed by the diffusive part, which is thus the reference. For the approximation solution, we use the KDMC simulation, but replace the diffusive motion with kinetic motions, which turns out to be another kinetic simulation with the fixed  $\Delta t$ . Then, we assume only the starting position of a diffusive step is known as the real diffusive motion, so that the fluid estimation described in Section 2.4 can be applied. In

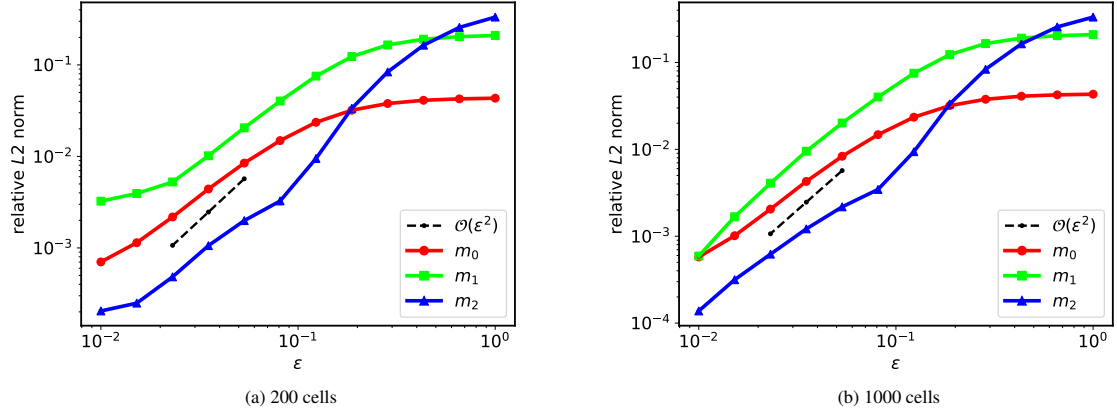


Figure 6: Model error  $\epsilon_m$  and discretization error  $\epsilon_{\Delta x}$ . From 200 cells to 1000 cells, the error of the  $m_1$  moment at  $\epsilon = 0.01$  decreases significantly, indicating the domination of the discretization error.

this setting, there is no propagated error  $\epsilon_i$ , since all particle movements follow the unbiased kinetic simulation. By scoring only the diffusive part, we get the separated error  $\epsilon_{\Delta t}$ , in terms of  $\Delta t$ .

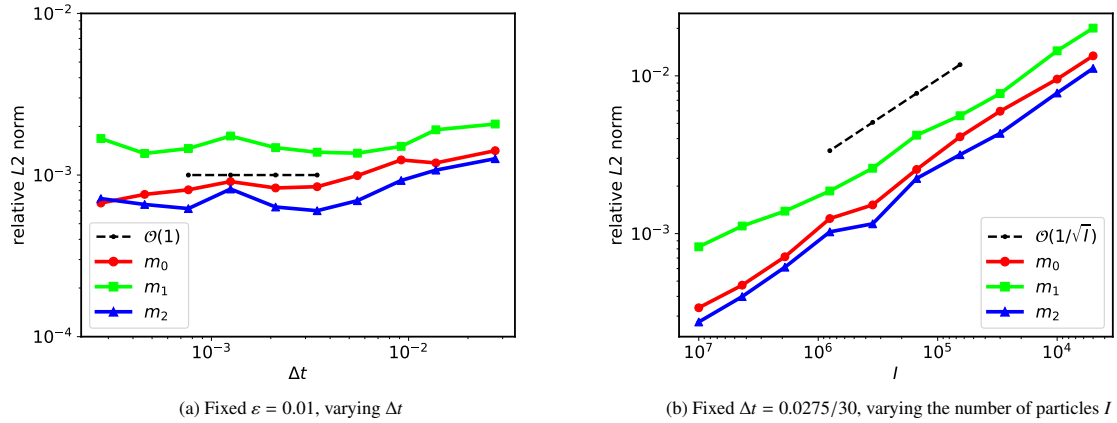


Figure 7: The time evolution error  $\epsilon_{\Delta t}$ . This error is of order  $O(1/\sqrt{N})$  and not depend on  $\Delta t$ .

The numerical results are displayed in Figure 7. Figure 7a presents the relative  $L_2$  error (57) between the constructed reference solution and the approximate solution described above as a function of the time step  $\Delta t$ . It shows that the error  $\epsilon_{\Delta t} = O(1)$  with respect to  $\Delta t$ , confirming that it is independent of the time step. Furthermore, plotting the error against the number of particles  $I$  in Figure 7b, we can see that  $\epsilon_{\Delta t} = \eta = O(1/\sqrt{I})$ . The two experiments confirm that  $\epsilon_{\Delta t}$  is purely a statistical error and does not depend on the choice of time step  $\Delta t$ .

#### 5.4.3. Diffusive error $\epsilon_d$

We have shown the components  $\epsilon_m$ ,  $\epsilon_x$ , and  $\epsilon_{\Delta t}$  of the diffusive part of the estimation error in Sections 5.4.1 and 5.4.2. Here, we illustrate this error  $\epsilon_d$  as defined in (39), and simultaneously examine the propagated error  $\epsilon_i$ . In (39), the approximate moment  $m^{kd,d}$  is the moment without scoring the kinetic part in KDMC. The reference moment  $(1 - \alpha)m^k$ , given by the kinetic method, is obtained by fixing the time step  $\Delta t$  and without scoring the first flight.

The estimation error of the diffusive part is provided in (53). For focusing on the effects of  $\Delta t$  and  $\epsilon$ , we employ a sufficiently large number of particles with  $I = 10^7$  and a spatial mesh with 200 grid cells, ensuring that both the statistical and discretization errors are negligible. Hence, only the model error  $\epsilon_m$  and the propagated error  $\epsilon_i$  remain significant. The error  $\epsilon_d$  is illustrated in Figure 8. Let  $\epsilon = 0.01$ , the error as a function of  $\Delta t$  is shown in Figure 8a.

The vertical dashed line indicates the point  $\Delta t = \varepsilon^2$ . It can be seen that the error scales as  $O(1/\Delta t)$  when  $\Delta t \gg \varepsilon^2$ , and as  $O(\Delta t)$  when  $\Delta t \ll \varepsilon^2$ , which displays the convergence behavior of  $\epsilon_i$  in (47) and confirms the existence of  $\epsilon_i$ , since other error components  $\epsilon_m$ ,  $\epsilon_x$ , and  $\epsilon_{\Delta t}$  do not have this shape of convergence. Next, we fix  $\Delta t = \bar{t}/5$  and plot the error against  $\varepsilon$  in Figure 8b. The error curves exhibit a similar shape to the model error displayed in Figure 6a, i.e., the error decreases only when  $\varepsilon$  is small. This indicates that the model error  $\epsilon_k$  dominates.

In Figure 8a, the error of the  $m_1$  moment does not decrease as  $O(\Delta t)$  in the regime  $\Delta t \ll \varepsilon^2$  due to the domination of the error in the reference solution given by the kinetic method. If a larger mean velocity  $u_p$  is used, the error of  $m_1$  will decrease, such as  $u_p = 100$  (see [34] for this case). The effect of  $u_p$  for the kinetic simulation is briefly mentioned in Section 4.2 and demonstrated in Section 5.3. To maintain consistency and avoid repetition, we still use the test case with  $u_p = 30$  as in the other experiments.

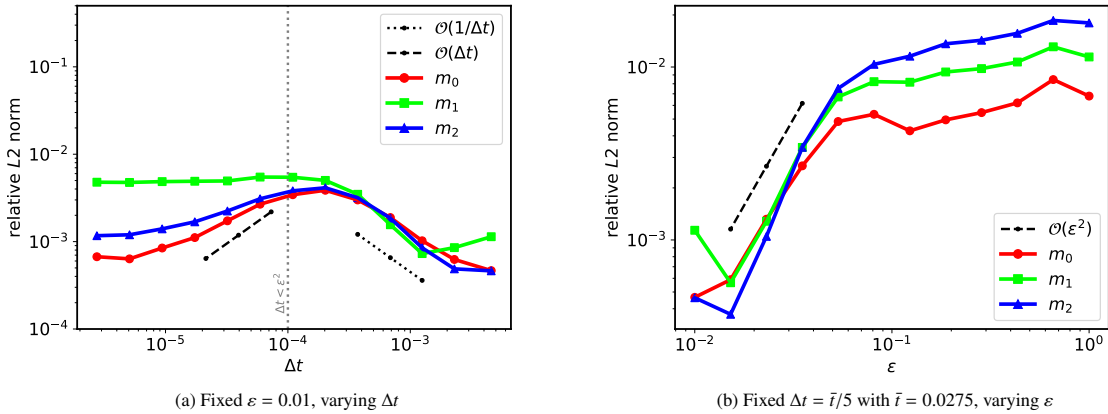


Figure 8: The diffusive part estimation error  $\epsilon_d$ .

### 5.5. Estimation error

We now present numerical results for the total estimation error of KDMC, defined in (38), with its error bound given in (54). The presentation is organized to separate the effects of the time step  $\Delta t$  and the diffusive scaling parameter  $\varepsilon$ . KDMC is expected to be more accurate than the fluid method described in Section 2.2, so the fluid method is compared in this experiment. The kinetic method is again the reference solution. In all plots, solid lines represent the estimation errors of KDMC, while dashed lines correspond to the errors of the fluid method. As before, red, green, and blue represent the error of  $m_0$ ,  $m_1$ , and  $m_2$  moments, respectively. The vertical dashed line indicates the point where  $\Delta t = \varepsilon^2$ .

In terms of the scaling parameter  $\varepsilon$ , the total estimation error  $\epsilon_{kd}(\varepsilon) = O(1/\varepsilon)$  when  $\Delta t \ll \varepsilon^2$ , and  $\epsilon_{kd}(\varepsilon) = O(\varepsilon^2)$  when  $\Delta t \gg \varepsilon^2$ . The corresponding convergence is shown in Figure 9, with  $K = \bar{t}/\Delta t = 1, 5, 25$ , and 75 time steps used in Figures 9a-9d, respectively. If the time step  $\Delta t$  is large such that  $\Delta t \gg \varepsilon^2$ , e.g., on the left side of the vertical line in Figures 9a and 9b, the diffusive part dominates KDMC, and the error convergence is of order  $O(\varepsilon^2)$ . Especially, if only one time step is used, i.e.,  $\Delta t = \bar{t}$ , the dashed lines and the solid lines coincide when  $\varepsilon \rightarrow 0$  since KDMC converges to the fluid method. If the time step  $\Delta t$  is small such that  $\Delta t \ll \varepsilon^2$ , e.g., on the right side of the vertical line in Figures 9c and 9d, the kinetic part dominates KDMC, and the error increases as  $O(1/\varepsilon)$ . Due to the domination of the kinetic part, where the fluid model (4) is not accurate, KDMC has a significantly lower error than the fluid method.

As for the time step  $\Delta t$ , the total estimation error  $\epsilon_{kd}(\Delta t) = O(\Delta t)$  when  $\Delta t \ll \varepsilon^2$ , and  $\epsilon_{kd}(\Delta t) = O(1/\Delta t)$  when  $\Delta t \gg \varepsilon^2$ . The convergence is displayed in Figure 10, with fixed values of  $\varepsilon = 0.1, 0.05, 0.02$ , and 0.01 shown in Figures 10a-10d, respectively. The dashed lines are flat, indicating that the error of the fluid method is independent of the time step. When  $\Delta t \ll \varepsilon^2$ , such as the left side of the vertical line in Figures 10a and 10b, the KDMC error converges with the order  $O(\Delta t)$ . When  $\Delta t \gg \varepsilon^2$ , such as the right side of the vertical line in Figures 10b and 10c, this error grows with the order  $O(1/\Delta t)$ . Note that this convergence is not immediately apparent, as the KDMC error is already low and close to the reference error level in this homogeneous test case, thereby obscuring the convergence.

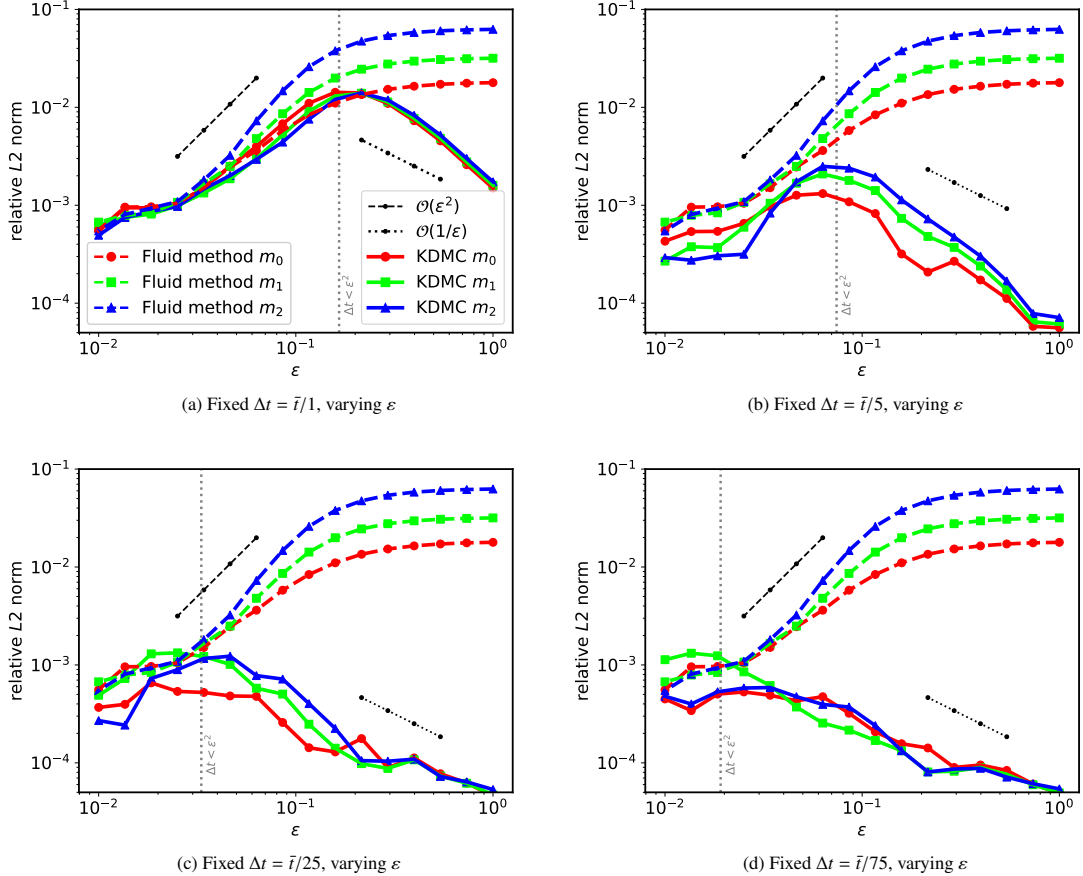


Figure 9: The total estimation error  $\varepsilon_{kd}$  as  $\varepsilon \rightarrow 0$ . The plots are arranged in row-major order with 1, 5, 25, and 75 time segments.

This convergence can be observed more clearly in the fusion-relevant heterogeneous test case in Section 5.6. Finally, when  $\varepsilon = 0.01$ , shown in Figure 10d, KDMC converges to the fluid model. Thus, the errors of both methods are close.

In conclusion, this experiment confirms our expectation that KDMC is more accurate than the fluid method, except in the high-collisional regime, where KDMC converges to the fluid solution and both methods exhibit similar levels of accuracy.

### 5.6. Fusion-relevant heterogeneous test case

The numerical experiments presented earlier are based on a homogeneous background. However, as explained in Section 4.1, if the moderate assumption  $R(x) = O(1/\varepsilon^2)$  is satisfied, the total estimation error (41) and further (54) also hold in a heterogeneous background. In this section, we demonstrate the effectiveness of KDMC and our analysis for the heterogeneous background using a fusion-relevant test case.

In the plasma edge region of a Tokamak, particles interact with the solid wall and undergo reflection, necessitating the use of reflective boundary conditions. However, the study of such boundary conditions within the KDMC framework is still an open research question, and we leave this question for future work. Therefore, we consider a test case that adopts the profile from a realistic fusion scenario [21], but employs the periodic boundary condition instead.

In this test case, the particle system is simulated on the periodic domain  $x \in [0, 1]$ , from  $t = 0$  s to  $\bar{t} = 0.001$  s. The initial density is given by  $\rho(x, t = 0) = 1 + 1/(2\pi) \times \sin(2\pi x)$  [ $\text{m}^{-1}$ ]. The variance of the plasma velocity and the collision rate are set to the values used in [21], namely,

$$\sigma_p^2(x) = \frac{eT_i(x)}{m_p} \quad [\text{m}^2\text{s}^{-2}], \quad \text{and} \quad R(x) = \rho_i \cdot 3.2 \times 10^{-15} \left( \frac{T_i(x)}{0.026} \right)^{1/2} \quad [\text{s}^{-1}], \quad (58)$$

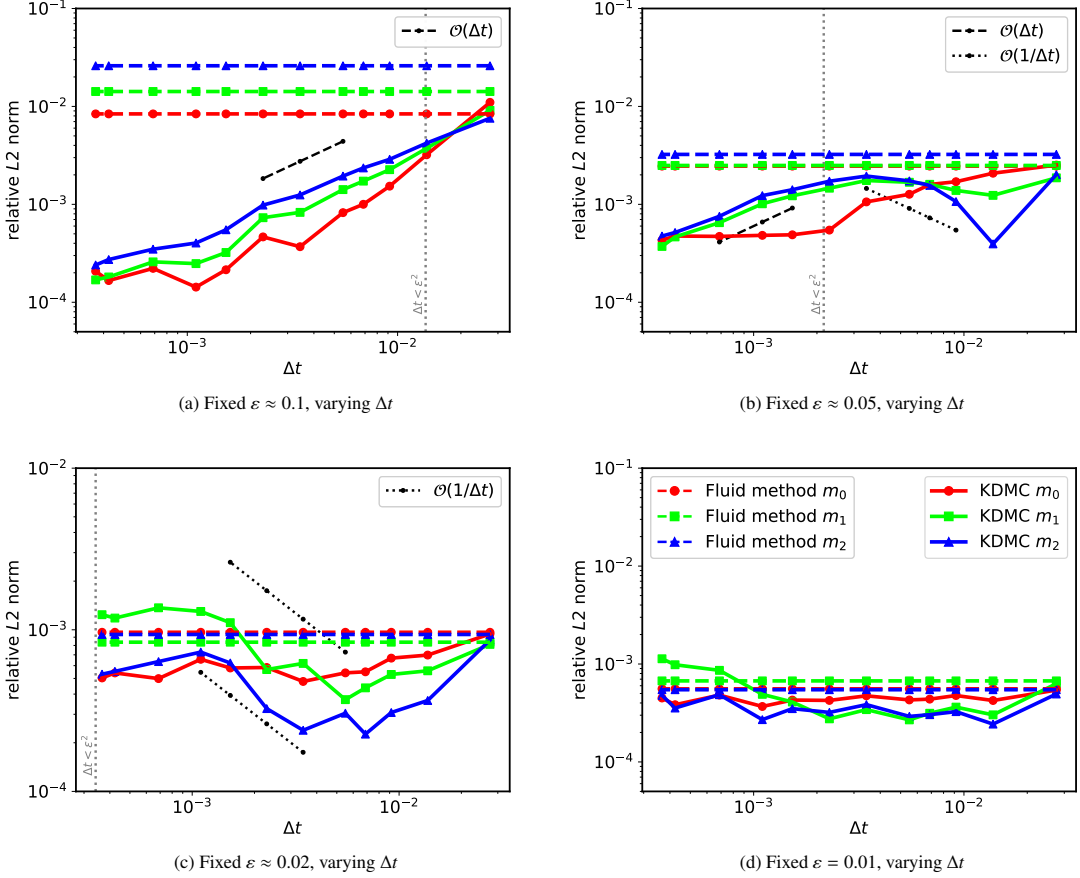


Figure 10: Total estimation error  $\epsilon_{kd}$  as  $\Delta t \rightarrow 0$ . The plots are arranged in row-major order for  $\epsilon \approx 0.1, 0.05, 0.02$ , and  $0.01$ . In subplot (b), the expected convergence rate of  $O(1/\Delta t)$  is less apparent, as the KDMC error is already low and close to the reference error level. Clear convergence behavior is observed in the fusion-relevant test case, as predicted by our theory.

where  $e \approx 1.60 \times 10^{-19} \text{ J-eV}^{-1}$  is the value of one electronvolt,  $m_p \approx 1.67 \times 10^{-27} \text{ kg}$  is the plasma particle mass, and  $T_i(x) = 5.5 + 4.5 \times \cos(2\pi x) \text{ [eV]}$  is the temperature of ions, which reaches  $10 \text{ eV}$  at the domain boundaries and equals  $1 \text{ eV}$  at the center of the domain. The meaning and units of the remaining constants can be found in [35]. The ion density  $\rho_i = 10^{21} \text{ m}^{-3}$  is a constant. The background (58) is modeled as being close to the limit in a diffusive scaling. To make this modeling assumption explicit, we introduce the scaled quantities

$$\tilde{\sigma}_p^2(x) = \frac{10^{-7}}{\epsilon^2} \sigma_p^2, \quad \text{and} \quad \tilde{R}(x) = \frac{10^{-7}}{\epsilon^2} R(x), \quad (59)$$

given that  $\sigma_p^2(x)$  and  $R(x)$  have an order of magnitude of  $10^7$ . In the experiment, we vary  $\epsilon$  from  $10^0$  to  $10^{-3.5}$ . Lastly, the mean plasma velocity is chosen as  $u_p(x) = 100 + 1/(6\pi) \times \sin(6\pi x) \text{ [ms}^{-1}\text{]}$ .

Using the kinetic method as a reference and the fluid method as the comparison, the convergence is displayed in Figure 11. The same color and line conventions apply as in Section 5.5. The point where the convergence changes in a homogeneous background is around  $\Delta t = 1/R \approx \epsilon^2$ . In this heterogeneous background, we choose this point as  $\Delta t = \text{mean}(1/\tilde{R}(x))$ , the mean of  $1/\tilde{R}(x)$ , indicated by the vertical dashed line.

Fixing the time step size  $\Delta t = \bar{t}/85$ , the error against the diffusive scaling parameter  $\epsilon$  is shown in Figure 11a. In this test case, the error of the fluid method (dashed lines) starts to converge only when  $\epsilon$  is around  $10^{-3}$ , while KDMC (solid lines) has smaller errors for all  $\epsilon$ . We see again, as in the homogeneous case in Section 5.5, that the total KDMC estimation error (solid lines)  $\epsilon_{kd}(\epsilon) = O(1/\epsilon)$  when  $\Delta t \ll \epsilon^2$ , and  $\epsilon_{kd}(\epsilon) = O(\epsilon^2)$  when  $\Delta t \gg \epsilon^2$  as predicted in (54). When  $\epsilon = 10^{-3.5}$ , which is the fusion test case in [21], KDMC outperforms the fluid model in terms of error by one

order of magnitude. In the non-high collisional regime, KDMC could be even more accurate. Note that the specific choice of the time step size  $\Delta t$  is made because the results are easier to interpret visually. The same convergence can be observed with other time step sizes (see more experiments at [34]).

Fixing  $\varepsilon = 0.0072$ , the error varying with  $\Delta t$  is illustrated in Figure 11b. The analytical convergence rate from (54) is clearly observable: when  $\Delta t \ll \varepsilon^2$ ,  $\epsilon_{kd}(\Delta t) = O(\Delta t)$ ; whereas when  $\Delta t \gg \varepsilon^2$ ,  $\epsilon_{kd}(\Delta t) = O(1/\Delta t)$ . For all choices of  $\Delta t$ , the error of KDMC is lower than that of the fluid method. Especially for  $\Delta t \geq 10^{-4}$ , the error of KDMC is more than one order of magnitude lower than that of the fluid method.

In conclusion, the performance of KDMC and the associated fluid estimation follows our analysis in Section 4. In the heterogeneous case, the analyzed algorithm outperforms the fluid method even in the high-collision regime.

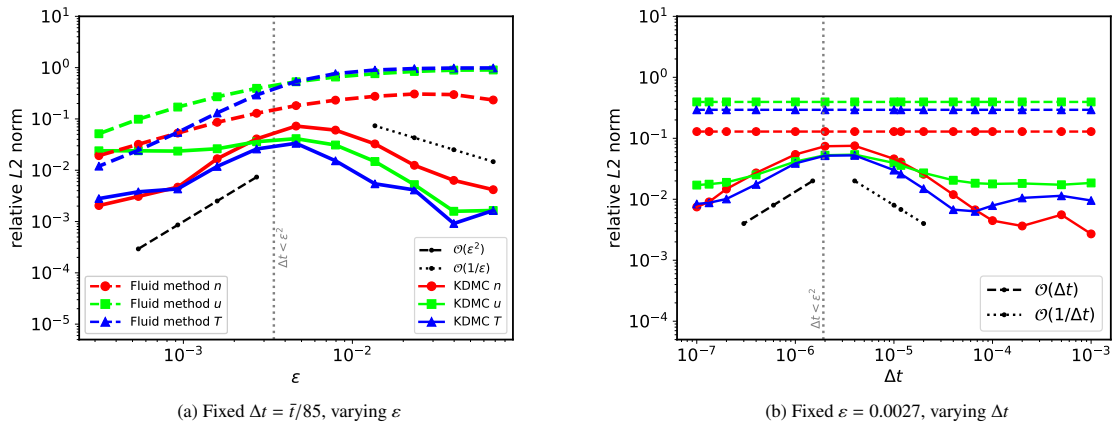


Figure 11: The total estimation error  $\epsilon_{kd}$  of the fusion-relevant test case.

### 5.7. Computational cost of KDMC

The KDMC method is expected to offer higher accuracy than the fluid model while being computationally more efficient than the kinetic method. The accuracy is demonstrated via the homogeneous test case in Section 5.5 and the fusion-relevant test case in Section 5.6. In this section, we discuss the computational cost.

We begin by analyzing the simulation stage when the trajectories of particles are generated. We assume the computational cost of a kinetic step (8) and a diffusive step (11) is comparable, as both steps first generate one or two random numbers and update the particle's position, as shown in Algorithm 1. Therefore, we treat each step as a unit computational operation. The kinetic simulation updates the position along with each collision. Thus, if we assume the collision rate  $R = 1/\varepsilon^2$ , the number of operations, denoted as  $C_k$ , is  $C_k = R\bar{t} = \bar{t}/\varepsilon^2$  with  $\bar{t}$  the simulation time and  $R\bar{t}$  the total number of collisions. KDMC has two positional updates in each  $\Delta t$ ; hence, the number of operations, denoted as  $C_{kd}$ , is  $C_{kd} = 2\bar{t}/\Delta t = 2K$ , where  $K$  is the number of time steps of size  $\Delta t$ . The KDMC simulation has fewer operations than the kinetic simulation if  $C_{kd} < C_k$ , which gives the condition  $\Delta t > 2\varepsilon^2$ . It indicates roughly the regime where the error of the diffusive part dominates. For instance, the left side of the vertical dashed line in Figure 11a, and the right side of it in Figure 11b.

When the estimation stage is included, moments in the kinetic method can be estimated concurrently with the simulation (see Algorithm 1), incurring negligible additional cost. As for KDMC, the fluid estimation is performed after the simulation. This estimation solves the fluid model (4) with the evolution time  $\hat{\theta}$  bounded by the time step  $\Delta t$ . In the meantime, the computational cost of solving the fluid model in the estimation stage is typically negligible compared with the cost of the KDMC simulation. Therefore, the computational cost is decided by the simulation stage in both the kinetic method and KDMC, and the speed-up achieved by using KDMC instead of the kinetic method is effectively quantified by the ratio of operations  $C_k/C_{kd} \approx \Delta t/\varepsilon^2$ .

Table 1 presents the computation time for the fusion-relevant test case introduced in Section 5.6, with  $\varepsilon = 0.0027$ , corresponding to Figure 11b. The first three columns display the number of time steps, the simulation time, and the estimation time measured in seconds, respectively. It is evident that the estimation time is negligible compared to the simulation time. The fourth column presents the speed-up, compared to the run-time of the reference kinetic method,

which is 48066.03 seconds. It can be readily verified that the speed-up is proportional to  $1/K$  with  $K$  the number of time steps. As  $K$  increases such that  $C_{kd} > C_k$ , that is,  $\Delta t = \bar{t}/K \leq 2\varepsilon^2$ , KDMC becomes less efficient, resulting in a slowdown indicated in the gray-highlighted rows of the table.

Table 1: Runtime of KDMC simulation with fluid estimation. Speed-up is computed by comparing the total KDMC runtime to that of the kinetic method (48066.03 seconds). Cases with a slowdown are highlighted in gray.

#time steps $K$	Simulation time (s)	Estimation time (s)	Speed-up
1	1216.29	0.111105	39.47
2	1874.68	0.052020	25.64
5	3637.70	0.020168	13.22
10	6686.51	0.011620	7.19
15	9701.11	0.006695	4.95
25	15758.76	0.004488	3.05
50	30865.44	0.002064	1.56
85	51739.55	0.001479	0.93
100	60388.68	0.001100	0.80

We finish this section by remarking that the test case above is performed in a one-dimensional problem in space. If a two- or three-dimensional case is considered, the computational cost of solving the fluid model in the estimation stage may be significant if a large  $\Delta t$  is used. Nevertheless, we expect that the cost of the KDMC simulation will still dominate. The analysis presented in this work can guide users in choosing an appropriate time step  $\Delta t$  for different application scenarios.

## 6. Conclusion

In this work, we analyze the KDMC method combined with a fluid estimation procedure. A fully kinetic Monte Carlo simulation is used as a reference, and a purely fluid model serves as a comparison. In addition to the asymptotic analysis, we conduct numerical experiments to verify the theoretical results. Homogeneous test cases are employed to assess each individual error, as well as the total error. Moreover, a fusion-relevant heterogeneous test case validates our analysis and the effectiveness of the analyzed algorithm for application-relevant problems.

In the first part of the analysis, we derive an error bound for the KDMC simulation based on the 1-Wasserstein distance. The error expression reveals the property that the KDMC simulation error remains low for both small and large diffusive scaling parameter  $\varepsilon$  (corresponding to the high- and low-collision regimes, respectively), but exhibits a relatively large bias in intermediate regimes. A similar property holds for the time step  $\Delta t$ : the error is low when  $\Delta t$  is either small or large, but relatively high in between. In particular, the bias reaches its peak around  $\Delta t = \varepsilon^2$ .

In the second part of the analysis, the estimation error is discussed. The estimation includes the kinetic part and the diffusive part. For the kinetic part, an unbiased MC estimator is used with only a statistical error. Besides the number of particles, this error is also affected by the time step size  $\Delta t$ , and the diffusive scaling parameter  $\varepsilon$ . We also observe that when the mean velocity of the background plasma is small, the statistical error of the  $m_1$  moment is larger than that of the  $m_0$  and  $m_2$  moments. For the diffusive part, the fluid estimation procedure is applied, which estimates the moments by solving the corresponding fluid model. The initial condition is constructed from the collection of all initial positions of the diffusive steps, while the evolution time is the average duration of all of these steps. This procedure introduces several sources of error, including stochastic and deterministic errors, each of which is analyzed both analytically and numerically.

To account for the mutual influence between the kinetic and diffusive parts, as well as the stochastic effect, dedicated experiments are designed to isolate and illustrate each individual error, confirming the validity of our analysis. As expected, KDMC is more accurate than the purely fluid method. Notably, in the fusion case, KDMC achieves an order of magnitude higher accuracy than the fluid method. Finally, the computational cost analysis shows that KDMC achieves a speedup over the kinetic method of a factor of  $\Delta t/\varepsilon^2$ , given that the cost of the fluid estimation is negligible.

This work provides a detailed analysis of KDMC and its associated fluid estimation. In future work, we plan to develop a multilevel scheme for the analyzed algorithm to accelerate the convergence. Moreover, we intend to derive a more accurate fluid model and integrate it into the KDMC framework to improve overall accuracy.

## Appendix A. Pseudo-time simulation

We compare two ways to simulate the steady-state Boltzmann-BGK equation

$$v\partial_x\phi(x, v) = -R_i(x)\phi(x, v) + R_{cx}(x)\left(\int_{-\infty}^{\infty}\phi(x, v')dv'\mathcal{M}(v) - \phi(x, v)\right) + S(x, v), \quad (\text{A.1})$$

by the time-dependent equation with the standard MC method, where the distribution  $\phi(x, v)$  is the steady-state solution.  $R_i(x)$  and  $R_{cx}(x)$  are the ionization and charge-exchange collision rates, respectively.  $S(x, v)$  is the source.

### Appendix A.1. Terminal-time simulation

The first way follows the pseudo-time stepping method [36]. Consider the time-dependent equation

$$\partial_t f(x, v, t) + v\partial_x f(x, v, t) = -R_i(x)f(x, v, t) + R_{cx}(x)\left(\mathcal{M}(v)\int_{-\infty}^{\infty}f(x, v', t)dv' - f(x, v, t)\right) + S(x, v), \quad (\text{A.2})$$

with the unknown  $f(x, v, t)$  and an initial guess  $f(x, v, t = 0)$ . The solution at a sufficiently large time  $t \approx \infty$ , denoted as  $f(x, v, \infty)$ , is the steady-state solution, that is,  $f(x, v, \infty) = \phi(x, v)$  the solution of (A.1). When the standard MC method is employed, we simulate the time-dependent equation (A.2) up to a sufficiently large terminal time  $\bar{t}$ , and estimate the steady-state distribution  $f(x, v, \bar{t})$  by recording the number of particles in each phase-space cell at time  $\bar{t}$ .

### Appendix A.2. Time-integrated simulation

Alternatively, we can define  $f(x, v, t)$  by

$$\int_0^{\infty}f(x, v, t)dt = \phi(x, v),$$

and solve

$$\partial_t f(x, v, t) + v\partial_x f(x, v, t) = -R_i(x)f(x, v, t) + R_{cx}(x)\left(\mathcal{M}(v)\int_{-\infty}^{\infty}f(x, v', t)dv' - f(x, v, t)\right), \quad (\text{A.3})$$

with the initial condition  $f(x, v, t = 0) = S(x, v)$  and the property

$$f(x, v, t = \infty) = 0, \quad (\text{A.4})$$

due to the sink term  $-R_i(x)f(x, v, t)$ . Integrating (A.3) over time  $t$  from 0 to  $\infty$ , we have

$$f(x, v, t = \infty) - f(x, v, t = 0) + v\partial_x\phi(x, v) = -R_i\phi(x, v) + R_{cx}(\mathcal{M}(v)\int_{-\infty}^{\infty}\phi(x, v')dv' - \phi(x, v)).$$

Substituting the initial condition  $S(x, v)$  and the property (A.4), we obtain

$$v\partial_x\phi(x, v) = -R_i(x)\phi(x, v) + R_{cx}(x)\left(\int_{-\infty}^{\infty}\phi(x, v')dv'\mathcal{M}(v) - \phi(x, v)\right) + S(x, v), \quad (\text{A.5})$$

which is exactly the steady-state equation (A.1) we want to solve. Hence, we can get  $\phi(x, v)$  by integrating  $f(x, v, t)$ , the solution of (A.3), over time  $t$ . When using the standard MC, we again simulate the time-dependent equation up to a sufficiently large time  $\bar{t}$ , but in this approach, we record the number of particles in each phase-space cell at all times from  $t = 0$  to  $\bar{t}$ . Compared with the MC method in Appendix A.1, which only records the number of particles at time  $\bar{t}$ , the MC method in this section scores more samples and therefore achieves a lower variance (or error). Moreover, although the latter improves statistical accuracy, it has almost the same computational cost as the former.

For the purpose of algorithmic analysis, we neglect the ionization term  $R_i(x)\phi(x, v)$ , since KDMC is designed for systems involving charge-exchange collisions only. The ionization process can instead be handled separately using an operator-splitting approach [37, 6]. As a result, the time-dependent equation (A.3) reduces to the Boltzmann-BGK equation (1) considered in this work.

## Appendix B. Mild formulation of Boltzmann-BGK equation

In this section, we derive the mild formulation [29] of the Boltzmann-BGK equation (1). The Boltzmann-BGK equation without the ionization term (1) reads

$$\partial_t f(x, v, t) + v \partial_x f(x, v, t) = R(M[f](x, v, t) - f(x, v, t)), \quad (\text{B.1})$$

with the initial condition

$$f(x, v, t = 0) = f_0(x, v),$$

where

$$M[f](x, v, t) = M_p(v|x) \int_{-\infty}^{\infty} f(x, v', t) dv'. \quad (\text{B.2})$$

and  $R$  the constant collision rate, since we consider a homogeneous background. Using the method of characteristics, Equation (B.1) can be written as

$$\frac{d}{dt} f(x(t), v, t) = R(M[f](x(t), v) - f(x(t), v)), \quad (\text{B.3})$$

along the path

$$x(t) = x(s) + v \cdot (t - s), \quad (\text{B.4})$$

where  $0 \leq s \leq t$  and we have

$$f(x(0), v, t = 0) = f_0(x(t) - vt, v). \quad (\text{B.5})$$

We solve the ODE (B.3) by first multiplying the factor  $e^{Rt}$  on both side of (B.3) which gives

$$e^{Rt} \frac{d}{dt} f(x(t), v, t) + R e^{Rt} f(x(t), v) = R e^{Rt} M[f](x(t), v, t).$$

Equivalently, we have

$$\frac{d}{dt} (e^{Rt} f(x(t), v, t)) = R e^{Rt} M[f](x(t), v, t). \quad (\text{B.6})$$

Then, integrating (B.6) over time from 0 up to  $t$  gives

$$e^{Rt} f(x(t), v, t) = f(x(0), v, 0) + \int_0^t R e^{Rs} M[f](x(s), v, s) ds. \quad (\text{B.7})$$

Substituting (B.2), (B.4) and (B.5) into (B.7), and rearranging terms, we obtain

$$f(x, v, t) = e^{-Rt} f_0(x - vt, v) + \int_0^t R e^{-R(t-s)} M(v|x - v(t-s)) \int_{-\infty}^{\infty} f(x - v'(t-s), v', s) dv' ds, \quad (\text{B.8})$$

the mild formulation of the Boltzmann-BGK equation without the ionization term (B.1). Note that if the heterogeneous background  $R = R(x)$  is considered, the derivation above still holds. We will have

$$f(x, v, t) = e^{\Lambda(t, 0; x, v)} f_0(x - vt, v) + \int_0^t R(x - v(t-s)) e^{\Lambda(t, s; x, v)} M[f](v|x - v(t-s)) ds,$$

with

$$\Lambda(t, 0; x, v) = \int_s^t R(x - v(\tau)) d\tau.$$

### Acknowledgements

This work has been carried out within the framework of the EUROfusion Consortium, funded by the European Union via the Euratom Research and Training Programme (Grant Agreement No 101052200 — EUROfusion). The views and opinions expressed herein do not necessarily reflect those of the European Commission. Part of this research was funded by the Research Foundation Flanders (FWO) under grant G085922N. Emil Løvbak was funded by the Deutsche Forschungsgemeinschaft (DFG, German Research Foundation) — Project-ID 563450842. The authors are also grateful to Vince Maes for valuable discussions.

## CRediT authorship contribution statement

**Zhirui Tang:** Conceptualization, Methodology, Software, Investigation, Visualization, Writing – Original Draft.  
**Julian Koellermeier:** Supervision, Writing – Review & Editing. **Emil Løvbak:** Supervision, Methodology, Validation, Writing – Review & Editing. **Giovanni Samaey:** Conceptualization, Supervision, Funding Acquisition, Writing – Review & Editing.

## Data availability

The data and source code that support the findings of this study are publicly available at: [https://gitlab.kuleuven.be/u0158749/kdmc\\_and\\_fluid\\_estimation\\_analysis](https://gitlab.kuleuven.be/u0158749/kdmc_and_fluid_estimation_analysis)

## References

- [1] O. N. Vassiliev, Monte Carlo Methods for Radiation Transport, Biological and Medical Physics, Biomedical Engineering, Springer International Publishing, Cham, 2017. doi:10.1007/978-3-319-44141-2.
- [2] C. Cercignani, Rarefied Gas Dynamics: From Basic Concepts to Actual Calculations, Cambridge Texts in Applied Mathematics, Cambridge University Press, Cambridge ; New York, 2000.
- [3] D. Borodin, F. Schluck, S. Wiesen, D. Harting, P. Börner, S. Brezinsek, W. Dekeyser, S. Carli, M. Blommaert, W. Van Uytven, M. Baelmans, B. Mortier, G. Samaey, Y. Marandet, P. Genesio, H. Bufferand, E. Westerhof, J. Gonzalez, M. Groth, A. Holm, N. Horsten, H. Leggate, Fluid, kinetic and hybrid approaches for neutral and trace ion edge transport modelling in fusion devices, Nucl. Fusion 62 (2022) 086051. doi:10.1088/1741-4326/ac3fe8.
- [4] P. C. Stangeby, The Plasma Boundary of Magnetic Fusion Devices, Plasma Physics Series, Institute of Physics Pub, Bristol ; Philadelphia, 2000.
- [5] H. G. Othmer, T. Hillen, The Diffusion Limit of Transport Equations Derived from Velocity-Jump Processes, SIAM J. Appl. Math. 61 (2000) 751–775. doi:10.1137/S0036139999358167.
- [6] V. Maes, W. Dekeyser, J. Koellermeier, M. Baelmans, G. Samaey, Hilbert expansion based fluid models for kinetic equations describing neutral particles in the plasma edge of a fusion device, Physics of Plasmas 30 (2023) 063907. doi:10.1063/5.0146158.
- [7] J. D. Densmore, T. J. Urbatsch, T. M. Evans, M. W. Buksas, A hybrid transport-diffusion method for Monte Carlo radiative-transfer simulations, Journal of Computational Physics 222 (2007) 485–503. doi:10.1016/j.jcp.2006.07.031.
- [8] N. Crouseilles, P. Degond, M. Lemou, A hybrid kinetic/fluid model for solving the gas dynamics Boltzmann–BGK equation, Journal of Computational Physics 199 (2004) 776–808. doi:10.1016/j.jcp.2004.03.007.
- [9] P. Degond, G. Dimarco, Fluid simulations with localized boltzmann upscaling by direct simulation Monte-Carlo, Journal of Computational Physics 231 (2012) 2414–2437. doi:10.1016/j.jcp.2011.11.030.
- [10] G. Dimarco, L. Pareschi, Hybrid Multiscale Methods II. Kinetic Equations, Multiscale Model. Simul. 6 (2008) 1169–1197. doi:10.1137/070680916.
- [11] N. Horsten, G. Samaey, M. Baelmans, A hybrid fluid-kinetic model for hydrogenic atoms in the plasma edge of tokamaks based on a micro-macro decomposition of the kinetic equation, Journal of Computational Physics 409 (2020) 109308. doi:10.1016/j.jcp.2020.109308.
- [12] A. Y. Aydemir, A unified Monte Carlo interpretation of particle simulations and applications to non-neutral plasmas, Physics of Plasmas 1 (1994) 822–831. doi:10.1063/1.870740.

[13] E. Gabetta, L. Pareschi, G. Toscani, Relaxation Schemes for Nonlinear Kinetic Equations, *SIAM J. Numer. Anal.* 34 (1997) 2168–2194. doi:10.1137/S0036142995287768.

[14] M. Bennoune, M. Lemou, L. Mieussens, Uniformly stable numerical schemes for the Boltzmann equation preserving the compressible Navier–Stokes asymptotics, *Journal of Computational Physics* 227 (2008) 3781–3803. doi:10.1016/j.jcp.2007.11.032.

[15] C. Buet, S. Cordier, An asymptotic preserving scheme for hydrodynamics radiative transfer models: Numerics for radiative transfer, *Numer. Math.* 108 (2007) 199–221. doi:10.1007/s00211-007-0094-x.

[16] G. Dimarco, L. Pareschi, High order asymptotic-preserving schemes for the Boltzmann equation, *Comptes Rendus Mathematique* 350 (2012) 481–486. doi:10.1016/j.crma.2012.05.010.

[17] B. Mortier, M. Baelmans, G. Samaey, A Kinetic-Diffusion Asymptotic-Preserving Monte Carlo Algorithm for the Boltzmann-BGK Model in the Diffusive Scaling, *SIAM J. Sci. Comput.* 44 (2022) A720–A744. doi:10.1137/20M1381526.

[18] L. Pareschi, G. Russo, Time Relaxed Monte Carlo Methods for the Boltzmann Equation, *SIAM J. Sci. Comput.* 23 (2001) 1253–1273. doi:10.1137/S1064827500375916.

[19] E. Løvbak, G. Samaey, S. Vandewalle, A multilevel Monte Carlo method for asymptotic-preserving particle schemes in the diffusive limit, *Numer. Math.* 148 (2021) 141–186. doi:10.1007/s00211-021-01201-y.

[20] E. Løvbak, G. Samaey, Accelerated Simulation of Boltzmann-BGK Equations near the Diffusive Limit with Asymptotic-Preserving Multilevel Monte Carlo, *SIAM J. Sci. Comput.* 45 (2023) A1862–A1889. doi:10.1137/22M1498498.

[21] N. Horsten, W. Dekeyser, G. Samaey, M. Baelmans, Comparison of fluid neutral models for one-dimensional plasma edge modeling with a finite volume solution of the Boltzmann equation, *Physics of Plasmas* 23 (2016) 012510. doi:10.1063/1.4940309.

[22] B. Mortier, Advanced Monte Carlo Simulation and Estimation for Kinetic Neutral Particles in the Plasma Edge of Fusion Reactors, Ph.D. thesis, KU Leuven, 2020.

[23] B. Mortier, V. Maes, G. Samaey, Estimation as a post-processing step for random walk approximations of the boltzmann-bgk model, *Contributions to Plasma Physics* 62 (2022). doi:10.1002/ctpp.202100197.

[24] D. Reiter, M. Baelmans, P. Börner, The EIRENE and B2-EIRENE Codes, *Fusion Science and Technology* 47 (2005) 172–186. doi:10.13182/FST47-172.

[25] S. Harris, An Introduction to the Theory of the Boltzmann Equation, Dover Books on Physics, Dover Publications, Mineola, N.Y., 2004.

[26] B. Lapeyre, É. Pardoux, R. Sentis, *Introduction to Monte-Carlo Methods for Transport and Diffusion Equations*, Oxford University PressOxford, 2003. doi:10.1093/oso/9780198525929.001.0001.

[27] I. Lux, L. Koblinger, *Monte Carlo Particle Transport Methods: Neutron and Photon Calculations*, 1 ed., CRC Press, 2018. doi:10.1201/9781351074834.

[28] C. Villani, *Optimal Transport: Old and New*, number 338 in *Grundlehren Der Mathematischen Wissenschaften*, Springer, Berlin, 2009.

[29] R. J. DiPerna, P. L. Lions, On the Cauchy Problem for Boltzmann Equations: Global Existence and Weak Stability, *The Annals of Mathematics* 130 (1989) 321. doi:10.2307/1971423. arXiv:1971423.

[30] V. M. Panaretos, Y. Zemel, Statistical Aspects of Wasserstein Distances, *Annu. Rev. Stat. Appl.* 6 (2019) 405–431. doi:10.1146/annurev-statistics-030718-104938.

- [31] T. H. Gronwall, Note on the Derivatives with Respect to a Parameter of the Solutions of a System of Differential Equations, *The Annals of Mathematics* 20 (1919) 292. doi:10.2307/1967124. arXiv:1967124.
- [32] K. Ghoos, W. Dekeyser, G. Samaey, P. Boerner, M. Baelmans, Accuracy and convergence of coupled finite-volume/Monte Carlo codes for plasma edge simulations of nuclear fusion reactors, *Journal of Computational Physics* (2016). doi:10.1016/j.jcp.2016.06.049.
- [33] M. Baeten, K. Ghoos, M. Baelmans, G. Samaey, Analytical study of statistical error in coupled finite-volume/Monte Carlo simulations of the plasma edge, *Contributions to Plasma Physics* 58 (2018) 659–665. doi:10.1002/ctpp.201700177.
- [34] Z. Tang, Python code for this paper, [https://gitlab.kuleuven.be/numa/public/kdmc\\_and\\_fluid\\_estimation\\_analysis](https://gitlab.kuleuven.be/numa/public/kdmc_and_fluid_estimation_analysis), 2025.
- [35] E. Løvbak, Multilevel and Adjoint Monte Carlo Methods for Plasma Edge Neutral Particle Models, Ph.D. thesis, KU Leuven, 2023.
- [36] C. T. Kelley, D. E. Keyes, Convergence Analysis of Pseudo-Transient Continuation, *SIAM J. Numer. Anal.* 35 (1998) 508–523. doi:10.1137/S0036142996304796.
- [37] S. MacNamara, G. Strang, Operator Splitting, in: R. Glowinski, S. J. Osher, W. Yin (Eds.), *Splitting Methods in Communication, Imaging, Science, and Engineering*, Springer International Publishing, Cham, 2016, pp. 95–114. doi:10.1007/978-3-319-41589-5\_3.